UNIVERSITÀ DEL PIEMONTE ORIENTALE

University of eastern Piedmont
"Amedeo Avogadro"
School of Medicine
Department of Health Sciences

**Master's degree course in MEDICAL BIOTECHNOLOGIES**

# Understanding the role of Glutaminase as a potential target to sensitize resistant Glioblastoma tumor initiating cells toward LSD1-directed therapy

Supervisor: **Prof. PELICCI Giuliana**

Co-supervisor: **COSTANZI Eva**

Candidate: **PUTZU Alice**
Matricula Number: **20030383**

Academic year: *2023/2024*

## INDEX

# 1. SUMMARY

Glioblastoma (GBM) is the most aggressive brain tumor, presenting significant challenges due to its molecular complexity and treatment resistance. Diagnosis via neuroimaging and biopsy has low specificity and sensitivity and involves surgical risks. Standard treatments fail due to inter- and intra-patient tumor diversity, low drug permeability through the blood-brain barrier (BBB), and the presence of tumor initiating cells (TICs). TICs, which have stem-like properties and survive in various GBM microenvironments, contribute to GBM malignancy. They play a crucial role in tumor initiation and progression, adapting to evade drug treatment and leading to disease recurrence. TICs' plasticity is under the control of epigenetic modifications that regulate the expression of metabolic genes. Recent findings have shown that inhibiting the epigenetic factor lysine-specific demethylase 1 (LSD1) reduces the proliferation and self-renewal of TICs *in vitro* and *in vivo*. In line with the GBM intertumor heterogeneity, a cohort of patient-derived TICs displayed resistance toward LSD1i (LSD1i$^{res}$ GBM-TICs). We hypothesize that metabolic modifications regulated by the interplay between epigenetic and metabolic processes may dictate the survival of LSD1i$^{res}$ GBM-TIC. A high-throughput shRNA screening identified glutaminase (GLS) as a driver for LSD1i resistance.

Our goal is to assess the intrinsic differences between LSD1i-sensitive and resistant TICs and understand the role of GLS in enabling resistant cells to overcome LSD1i therapy. Inhibiting GLS in LSD1i$^{Res}$ TICs might sensitize them to LSD1i by altering their metabolism.

We observed that GLS silencing in LSD1i$^{Res}$ TICs using shRNAs reduced GLS protein expression in shGLS cells, leading to impaired cell proliferation beyond the effects of LSD1i alone. Additionally, we tested the effect of a potent, selective, and orally bioavailable GLS inhibitor named Telaglenastat (CB-839).

We observed dose-dependent suppression of cell growth in LSD1i$^{res}$ TICs, when treated with CB-839. Pharmacological inhibition of GLS with CB-839 induced apoptosis in LSD1i$^{sens}$ and LSD1i$^{res}$ GBM-TICs.

Our study highlights the critical role of GLS in the metabolic adaptation of GBM-TICs, especially those resistant to LSD1i. Targeting GLS, either alone or combined with LSD1i, offers a promising strategy to disrupt the metabolic flexibility that supports tumor growth and resistance. These results suggest a combinatorial treatment of CB-839 and LSD1i as a therapeutic approach to bypass LSD1i resistance in GBM to be tested *in vivo*.

# 2. INTRODUCTION

## 2.1. Glioblastoma

Cancer is a major cause of death globally, responsible for nearly 10 million deaths in 2020, according to the World Health Organization (WHO, 2022). The Global Cancer Observatory (GLOBOCAN) reported in 2020 that brain and central nervous system (CNS) tumors are the 19th most common cancers (making up 1.9% of all cancers) and the 12th leading cause of cancer-related deaths (accounting for 2.5% of all cancer deaths). Gliomas, the most prevalent type of CNS tumors, originate from glial cells and are known for their invasive behavior that quickly impacts surrounding healthy brain tissue.[1]

Specifically, glioblastoma multiforme (GBM) is the most common and aggressive CNS tumor, representing 14.5% of all CNS tumors and 48.6% of malignant CNS tumors.[1]

GBM affects people of all ages and genders, with a higher incidence in adult males[2], and is more frequently diagnosed in Western countries[3]. This higher frequency is likely due to under-reporting in less developed countries[4], limited healthcare access, and differences in diagnostic practices.

The incidence of brain tumors increased by 1-2% annually during the 1980s and 1990s, coinciding with advancements in the diagnosis of neurological diseases through high-resolution neuroimaging[4].

Currently, there is limited understanding of the potential carcinogenic factors that may contribute to gliomas' development. No definitive link has been found between GBM and environmental factors such as smoking, diet, or electromagnetic fields[3].

For example, routine exposure to diagnostic radiation does not appear to increase the risk of developing GBM. Some studies suggest that immune responses during infections and allergic diseases may offer some protection against GBM[5,6].

Genetic predisposition accounts for 5-10% of glioma cases. [7] Certain rare genetic syndromes, including neurofibromatosis 1 and 2, tuberous sclerosis, retinoblastoma (RB) 1, Li-Fraumeni syndrome, and Turcot's syndrome, are associated with a higher risk of glioma, though they account for only a few cases. Gliomas can also occur in families without these syndromes, but the specific genes responsible for this familial susceptibility have not yet been identified.

GBM develops from the malignant transformation of cells, primarily astrocytes, in the brain or spinal cord.

The temporal lobe is the most common site for the primary tumor [8], while few tumors are found in the cerebellum, brainstem, and spinal cord[9].

Macroscopically, GBM appears as a large, irregular lesion with areas of hemorrhage, necrosis, and cysts[10].

Histologically, GBM is characterized by a diverse population of cells, including small, poorly differentiated tumor cells and large multinucleated cells with high mitotic activity.[3]

Another common feature of GBM lesions is the proliferation of vascular endothelial cells with glomeruloid structures[10].

### 2.2.1. GBM classification

The latest guidelines for glioma classification were issued in 2021 by the World Health Organization (WHO). They categorize gliomas into grades 1 to 4 based on clinicopathological, histological, and molecular characteristics [11] [12].

The 2021 update of the WHO classification for CNS tumors has significantly revised how these tumors are classified. One major change is the separation of GBM with isocitrate dehydrogenase (IDH) mutations into distinct categories, eliminating the option to label entries as "not otherwise specified" (NOS). This change refines the GBM category to include only the most aggressive tumors typically found in adults.[13]

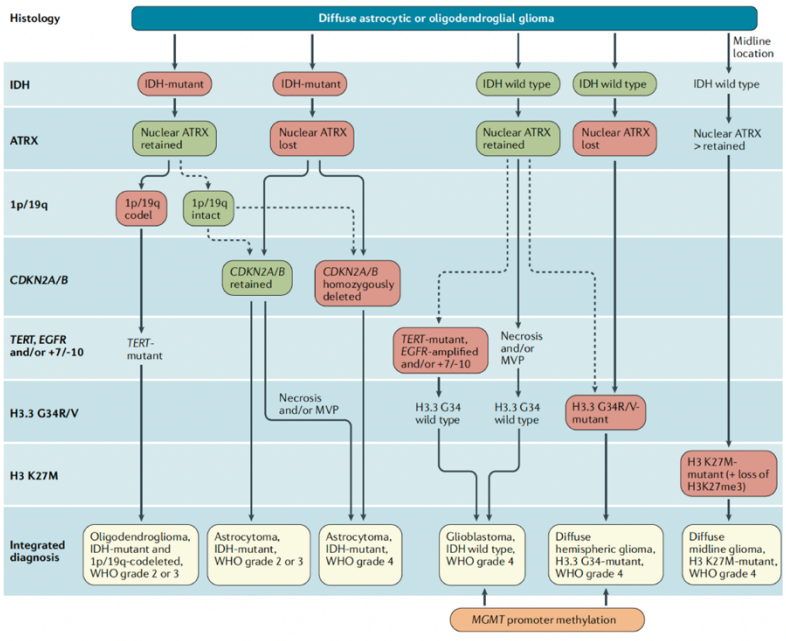


**Figure 1** ***A seven-layers approach for the classification of diffuse gliomas in adults****. For an integrated glioma diagnosis, a 7-layers structure combines histological features, grading, and molecular information. The presence and absence of the diagnostically most relevant molecular alterations for each tumor type are highlighted in green and red. According to the WHO classification, gliomas are classified and graded on scale 2-4 with increasing malignancy. Image from Brat, D.J. et al.,2022* [14]

### 2.2.2. Genetic factors involved in GBM classification

The latest classification for CNS tumors by WHO now clearly distinguishes between adult- and pediatric-type gliomas, recognizing their unique molecular characteristics and prognostic implications. This revision has led to a more accurate categorization of adult-type diffuse gliomas into three main groups: astrocytoma, characterized by IDH mutations; oligodendroglioma, defined by both IDH mutations and the co-deletion of chromosomes 1p and 19q; and GBM, which is now specifically linked with the absence of IDH mutations (IDH wild type). This change underscores the critical role of IDH mutation status in CNS tumor classification, limiting GBM diagnosis to IDH wild type tumors. Tumors previously identified as GBM with IDH mutations are now reclassified as grade 4 IDH-mutated astrocytoma. Additionally, the presence of IDH mutations has become a requisite for diagnosing tumors as either astrocytomas or oligodendrogliomas[15].

These significant updates primarily hinge on IDH mutations. This includes limiting the diagnosis of glioblastoma exclusively to IDH wild-type tumors, redefining tumors previously identified as IDH-mutant GBM as grade 4 IDH-mutant astrocytomas and mandating the presence of IDH mutations for the classification of tumors as either astrocytomas or oligodendrogliomas.

GBM is now defined as a diffuse astrocytic glioma without mutations in either IDH or H3 genes and is identified by one or more of the following features: microvascular proliferation, necrosis, mutations in the telomerase reverse transcriptase (TERT) promoter, amplification of the epidermal growth factor receptor (EGFR) gene, or a simultaneous gain of chromosome 7 and loss of chromosome 10 (+7/-10), qualifying it as a CNS WHO grade 4 tumor[16,17].

Traditional histological criteria for diagnosis GBM include identifying either necrosis or microvascular proliferation, termed histological GBM (hist-GBM). Meanwhile, IDH-wildtype diffuse astrocytic tumors lacking these histological markers, which might previously have been labeled as grade 2 or 3, are now recognized as molecular GBM (mol- GBM, WHO grade 4) when they exhibit specific molecular features such as mutations in the TERT promoter, EGFR gene amplification, or the +7/-10 chromosomal alteration [18,19]

Additionally, methylation data analysis can reveal changes in copy numbers, including the 1p/19q co-deletion, the distinct pattern of chromosome 7 gain and chromosome 10

loss (+7/-10), gene amplifications, complete gene deletions, and evidence of gene fusions[12].

Prognostic factors such as older age, male sex, tumors located in crucial or deep brain areas, and genetic mutations in CDK4, CDK6, CIC, FGFR3, KMT5B, and MYB are associated with worse outcomes, whereas methylation of the MGMT promoter is linked to better survival rates[20].

#### 2.2.3. Other Factors

The WHO uses a grading system to assess the malignancy of tumors based on four main histological features: nuclear atypia (A), mitotic figures (M), microvascular proliferation (E, previously known as endothelial proliferation), and necrosis (N).

These criteria are collectively referred to the acronym 'AMEN' score. To classify a tumor as grade 3, there must be significant mitotic activity, indicating a high rate of cell division. For a tumor to be classified as grade 4, the highest malignancy grade, it must show either microvascular proliferation, which is the formation of new blood vessels to sustain rapid tumor growth, or necrosis, which is the presence of dead tissue within the tumor due to insufficient blood supply. These features are commonly associated with GBM[21].

### 2.3. GBM diagnosis and treatment

The clinical presentation of GBM includes symptoms such as focal neurological deficits, increased intracranial pressure, and seizures.

In rare cases (less than 2%), patients may experience stroke-like symptoms due to bleeding within the tumor. Diagnosis is typically performed using Magnetic Resonance Imaging (MRI), followed by molecular profiling of a tissue biopsy. GBM is often identified at advanced stages when the brain lesion has already grown significantly, and tumor cells have spread into surrounding normal tissue.

Patients diagnosed with GBM undergo a standardized treatment regimen which includes maximally safe surgical resection to reduce its size, followed by a combination of the chemotherapy with drug temozolomide (TMZ) and radiotherapy, with additional TMZ treatment afterward [22].

The treatment aims to reduce the volume of the tumor, control its growth, and alleviate symptoms. However, several major characteristics of GBM hinder the effectiveness of this standard approach:

- some tumors are in critical areas of the brain and cannot be surgically removed.

- GBM tumor cells infiltrate surrounding brain tissue, making complete surgical removal challenging, leading to residual disease and recurrence[23].
- the presence of the blood brain barrier (BBB) limits the delivery of chemotherapeutic drugs to the brain, reducing their effectiveness.
- GBM tumors display extensive inter- and intra-patient heterogeneity and molecular dynamism. Thus, standardized therapeutic approaches fail to target the high genetic complexity of cells that constitute the tumor mass.
- GBM cells can adapt and reprogram in response to drug treatment due to their intrinsic plasticity and adaptable epigenetic profile[24,25.]

As a result, treatments are palliative rather than curative, and 90% of GBM patients experience disease relapse. The median overall survival of GBM patients is 15-18 months, and the 5-year survival rate is 6.6%, one of the lowest among human cancers. [26]
Many clinical trials are ongoing to explore novel treatments and therapies for GBM. These trials may involve targeted therapies, immunotherapies, or other experimental approaches.[27]
Clinical trials are underway to test novel treatments and combinations that may improve outcomes for GBM patients.

### 2.4. GBM heterogeneity

Despite the promising potential of molecular classification for GBM, Sottoriva et al.[28] found it inadequate for tailoring effective treatments due to the coexistence of different GBM subtypes within the same tumor, as revealed by Fluorescence-Guided Multiple Sampling (FGMS). Advancements in technologies like single-cell RNA sequencing (scRNA-seq) have enabled researchers to delve deeper into the complexity of GBM.
Patel and colleagues, for instance, identified that within the tumor bulk there was the coexistence of a variety of different type of tumor cells ranging from a more stem- like to a more differentiated phenotype, supporting the idea of a hierarchal organization. [29]
Furthermore, Couturier *et al.* confirmed this hypothesis by showing that tumor cells recapitulated the hierarchical organization of normal human neurodevelopment characterized by the presence of three neurodevelopmental lineages deriving from glial progenitor-like cells. These cells showed the potential to differentiate into astrocytic, neuronal and oligodendrocyte populations and to be more resistant to the chemotherapeutic agent temozolomide[29]. Instead, Neftel and collaborators identified distinct cellular states within GBM, such as neural-progenitor-like (NPC-like),

oligodendrocyte-progenitor-like (OPC-like), astrocyte-like (AC-like), and mesenchymal-like (MES-like), each associated with specific genetic alterations.

Furthermore, they discovered that each of the four transcriptional subtypes efficiently formed tumors in xenograft models and recapitulated tumor heterogeneity with the capacity to reestablish subtype diversity with transitions between cell states, further highlighting cellular plasticity [30]. Bhaduri and colleagues demonstrated that GBM exhibits a diverse cellular makeup, with different subpopulations of cells resembling expression patterns found in glial and neuronal lineages at varying stages of development. These cellular subsets also displayed markers typical of glioma stem cells, indicating that the heterogeneity of GBM cells reflects developmental programs present in normal neurodevelopment, which are expressed differentially across various GBM cell types[31]. Delving deeper into the characterization of GBM heterogeneity, Guilhamon *et al.* proved three stem-like cell states consisting of reactive, constructive, and invasive states and each of them is driven by distinctive features such as inflammatory signaling, neuron and glial development, and angiogenesis signatures, respectively. Additionally, Guilhamon et al. identified the specific transcription factors crucial for maintaining these different states[32.] As already described, data highlight the fact that tumor microenvironment and immune system cells, such as macrophages/microglia, may play a pivotal role in shaping tumor cells phenotype toward therapy resistance [33].

Moreover, Richards *et al.* demonstrated that cells could be found along a transcriptional gradient from a “Developmental” state to an “Injury Response" state. The first group is characterized by high proliferation and express genes correlated to neurodevelopmental programs, including self-renewal and proliferation; while the second group express a more MES-like gene signature, indicative of hypoxia, reactive astrocytes and wound-healing response. Each one is sensitive to the inhibition of genes peculiar to their transcriptional state, suggesting that a combined therapy is needed. [34] Garofano *et al.* used a computational approach for unbiased identification of core biological traits of single cells and bulk tumors. They discovered four cell states defining specific subtypes characterized by attributes of either development, neuronal (NEU) and proliferative/progenitor (PPR), or metabolism, mitochondrial (MTC) and glycolytic/plurimetabolic (GPM).

Within the metabolic branch, MTC cells are selectively dependent on oxidative phosphorylation (OXPHOS) for energy production and are correlated with a better clinical outcome. In contrast, GPM cells are highly resistant to therapy because they can switch

among different metabolic pathways. Among the four GBM subtypes, MTC tumors are associated with better clinical outcome. This pathway-based classification provides additional information for therapeutic development for the first time focusing the attention on the cellular metabolic state as a point of vulnerability.[35] The presence of different tumor cell states within the same tumor could be attributed to varying genetic backgrounds, adaptations to the tumor microenvironment, and responses to therapy, adding complexity to the quest for targeted treatments in GBM.

### 2.5. GBM tumor initiating cells (TICs)

The explanation of GBM heterogeneity identifies two major cell populations within the tumor: the tumor initiating cells (TICs) and the non-stem counterpart. TICs are characterized by a high potential self-renewal, their tumorigenicity *in vivo* and their ability to switch to more differentiated states and establish a heterogeneous mass that resembles the tumor of origin[36]. Single-cell studies attributed to TICs most of the features that shape GBM single-cell studies have shown that TICs contribute significantly to the genetic, epigenetic, and metabolic diversity of GBM, indicating that they play a crucial role in the development, progression, and recurrence of the disease. This underscores the importance of completely eradicating TICs through targeted therapies.

Definitively characterizing TICs is difficult, but they generally share several markers with normal stem cells. Some markers commonly found in TICs include Prominin-1 (PROM1 or CD133), Stage-specific embryonic antigen-1 (SSEA1 or CD15), L1 cell adhesion molecule (L1CAM), and SRY-box transcription factor 2 (SOX2). [35]

However, there is no definitive and exclusive marker that identifies TICs.

Studies regarding the origin and fate of TICs are controversial. Likely, TICs arise from the accumulation of genetic and epigenetic mutations in progenitor cells and neural stem cells. These mutated cancer cells can differentiate into various lineages, and some of them retain their self-renewal potential. Most events occurring within the tumor niche are thought to be reversible, thus also differentiated cells could revert to a TIC state via dedifferentiation, thanks to the underlying epigenetic plasticity[37].

The resulting system is a mix of canonical hierarchical differentiation[38] and clonal evolution[39,40].

*In vitro*, TICs, cultured in serum-free medium, form multipotent clonal spheres, called neurospheres which exhibit the same cellular diversity and plasticity as the primary tumor.

This makes them an ideal model system for testing new drugs aimed at impairing TIC survival.

### 2.6. TICs metabolism

The conventional understanding of cancer cell metabolism, known as the Warburg effect, posits that tumors primarily use glycolysis for energy production, with minimal glucose oxidation in the mitochondrial citric acid cycle[41]. GBM, like other tumors, has been described as relying on glycolysis to produce energy[42]. To evaluate this dependence, various imaging-based analysis have been developed, such as Positron Emission Tomography (PET)-based diagnosis that assesses glucose uptake, which resulted to be not reliable due to the high glucose abundance in the brain [43].

In contrast, the high production of lactic acid by GBM allows for non-invasive differential diagnosis via magnetic resonance spectroscopy[44].

However, studies on intact human brain tumors and in mice bearing human GBM cells have been shown that their metabolism involves extensive glucose oxidation by pyruvate dehydrogenase (PDH) and the citric acid cycle (CAC or TCA), anaplerosis, and glutamine accumulation[45].

Interestingly, human GBM orthotopic tumors share similar metabolic features but possess different driver mutations[46] and IDH status[47,48]. A small subset among GBM patients (around 3%) relies specifically on oxidative phosphorylation due to the fibroblast growth factor receptor 3 and the transforming acidic coiled coil containing protein 3 (FGFR3-TACC3) oncogenic chromosomal translocation. This fusion protein promotes mitochondrial biogenesis and supports subsequent tumor growth[49,50].

GBM cells can be divided into fast-cycling cells, which rely on glycolysis and slow cycling cells, which depend on oxidative phosphorylation [51].

The slow dividing cells represent the TICs subpopulation and their dependency on mitochondrial metabolism for energy production and survival is supported by *in vitro* and *in vivo* studies[52,53].

The presence of cells using different metabolic pathways was confirmed by identifying a mitochondrial glioma stem cell subtype able to switch from oxidative phosphorylation to glycolysis after inhibition of oxidative phosphorylation, suggesting that these cells are able to adapt to metabolic stress. [53]

By genetic transformation of neural stem cells with the same oncogenic lesion, Saga *et al.* demonstrated that within the tumor bulk there are two types of clones that manifest

high rates of either glucose or oxygen consumption. They show similar clonogenicity, differentiation capacity and tumorigenicity *in vivo*. The differential expression of glycolytic enzymes discriminates between the two subpopulations[54]. Targeting glycolytic genes has been shown to improve the survival of mice engrafted with GBM patient-derived GBM stem-like cell lines.[55]

The maintenance of a stem-like phenotype is closely tied to energy production. For instance, targeting the mitochondrial inner membrane protease subunit 2 (IMP2), which binds to complex I and IV proteins, in glioma spheres model impaired survival and self-renewal capacity in cells that use oxidative phosphorylation as their primary energy source. [56]

Under stress conditions, the cooperation Sirtuin 3 (SIRT3) and TNF receptor associated protein 1 (TRAP1) leads to the enhancement of efficient mitochondrial respiration without the overproduction of reactive oxygen species (ROS) that contribute to loss of stemness and subsequent cell differentiation. [57]

These findings suggest that TICs are not dependent on one specific metabolic pathway and their survival could depend on their ability to exploit other available resources.

Genetic screen *in vivo* and *in vitro* in patient-derived three- dimensional glioma tumor spheres revealed that medium-chain acyl-CoA dehydrogenase (MCAD) is essential for maintaining homeostasis by oxidating medium fatty acid in the mitochondria preventing their accumulation. Targeting MCAD induces oxidative stress and damage in the mitochondrial structure leading to cell death. [58].

Together with Lin and colleagues, this study presents a significant role of fatty acid in GBM growth and could open new treatment opportunities[59].

Furthermore, glutamine (GLN) also plays a key role in GBM maintenance.

Oizel *et al.* divided GBM cells into $GLN^{High}$ and $GLN^{Low}$, based on metabolic plasticity and GLN utilization. $GLN^{High}$ GBM cells can produce Nicotinamide adenine dinucleotide (NADH) from a wide variety of oxidizable substrates, displaying a strong metabolic adaptability to their microenvironment. Conversely, $GLN^{Low}$ cells exhibit a strong dependency on glucose associated with a poor survival in the absence of glucose[60]

Recently, another metabolic pathway has been identified in GBM under glucose deprivation: the use of fructose, the second most abundant sugar in human blood. Since glucose and fructose coexist in the bloodstream under normal conditions, fructolysis is not essential in normal tissues, offering a promising therapeutic target for GBM[61].

### 2.7. Glutaminase

Glutaminase (GLS) is the first enzyme involved in glutaminolysis, a physiological cellular process where GLN undergoes hydrolytic deamidation to produce glutamate (GLU) and ammonium ions. The enzyme is widely distributed in mammalian tissues where it performs essential tissue-specific functions.[62]

GLS protein family members are encoded by two paralogous genes: GLS and GLS2, presumably originated from gene duplication of a common ancestor.[63,64]

Historically, glutaminases have been identified by a variety of names and symbols. The gene symbols, approved by the Human Genome Organisation (HUGO) for the two human isoforms are GLS and GLS2. Occasionally GLS1 is used interchangeably with GLS. In this thesis, we use GLS to refer to all protein derived from GLS, whereas KGA, GAC refer to the specific splice variants.

In humans, GLS gene is on chromosome 2, whereas GLS2 gene is on chromosome 12. The two enzymes differ in kinetic properties, protein structure, and tissue distribution (**Table1**)[65].

**Table 1 Comparison between GLS and GLS2**

| | GLS | GLS2 |
|---|---|---|
| **Genome location** | Chromosome 2 | Chromosome 12 |
| **Exon numbers** | 19 | 18 |
| **Sub-isoforms** | KGA (exons 1–14, 16–19)<br>GAC (exons 1–15) | GAB (exons 1–18)<br>LGA (exons 2–18) |
| **Molecular weight** | GAC (58 KD)<br>KGA (64 KD) | GAB (77 KD)<br>LGA (65 KD) |
| **Tissue distribution** | Brain, Kidney, Intestine, Lung, Heart, Muscle, Pancreas | Liver, Brain |
| **Subcellular localization** | mitochondria | nucleus |
| **GLU affinity** | high | low |
| **Inhibitory effect of GLU** | yes | no |
| **Pi dependence** | high | low |

Alternative splicing of GLS gene produces two isoforms: kidney-glutaminase (KGA) and C glutaminase (GAC).

KGA mRNA is formed by joining exons 1–14 and 16–19, whereas the alternatively spliced GAC transcript includes only the first 15 exons, omitting exons 16–19 (**Figure 2**)[66,67].

The two isoforms also differ in their localization. KGA is mainly found in the cytoplasm, instead GAC is located in mitochondria [68–70].

Casago *et al.* demonstrated that GAC is the most efficient isozymes in hydrolyzing glutamine in the presence of inorganic phosphate (Pi)[71] and is frequently up regulated in cancer cells[66,67].

Biochemical studies of the kidney-type isozyme reported that mitochondrial glutaminases are mostly found as inactive dimers within the organelle. The presence of Pi induces changes that promote tetramerization and enzyme activation [70].

GLS2, which consist of 18 exons [64], has two identified L-type transcripts: the canonical long transcript termed GAB (long-transcript isoform), including all 18 exons of the gene and the short transcript LGA, which lacks exon 1 and was originally identified in rat liver (**Figure 2**)[64].

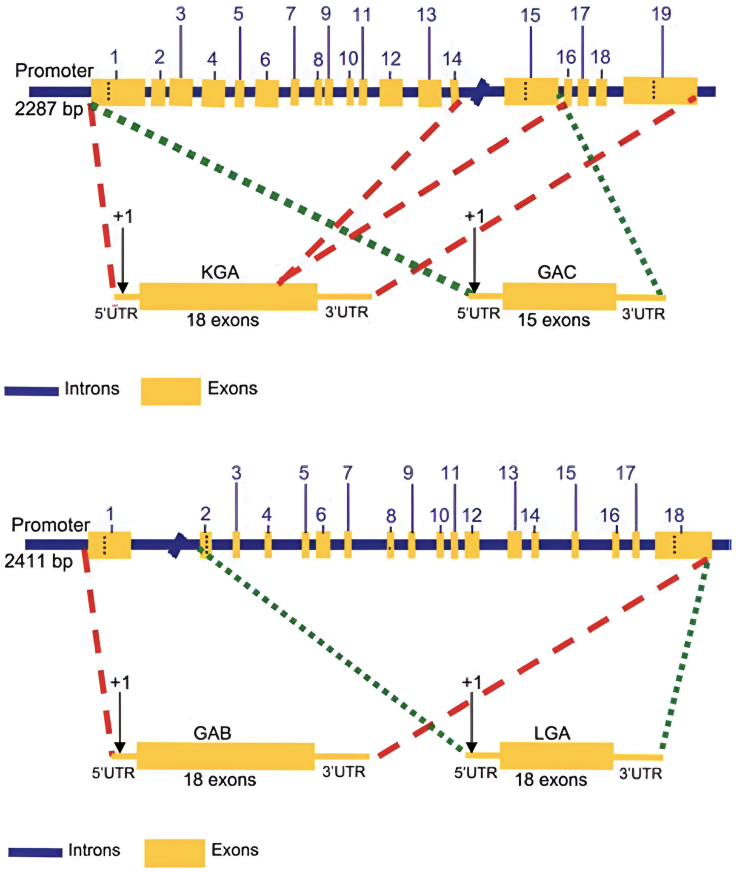


**Figure 2** ***Human GLS genes and mRNA transcripts.***
*(Top panel) Human glutaminase gene and alternative transcripts KGA and GAC. (Bottom panel) Human glutaminase 2 gene and transcripts GAB and LGA. Each gene is shown with introns depicted as solid blue lines and exons as numbered yellow boxes. The promoter regions are also indicated on the 59-end of each gene. Dashed red lines indicate the exons forming KGA and GAB mRNA transcripts, whereas dotted green lines comprise exons involved in the generation of transcripts GAC and LGA. The transcription start site is marked by an arrow and numbered as q1. Image from Marquez et al., 2010.*[62]

### 2.8. GLS and GLN metabolism in cancer

Upregulation of the GLS gene is observed in various cancers, including breast, liver, colorectal, brain, cervical, lung, and melanoma[72,73].

GLS and GLS2 play opposing roles in tumorigenesis: GLS interacts with oncogenes and promotes tumorigenesis, by contrary GLS2 acts as a tumor suppressor gene.

Furthermore, it has been demonstrated that cancer cells exhibit an upregulation of GAC compared to normal cells [74–77].

More in details, GLS is regulated by several signaling pathways, many of which are frequently dysregulated in cancer and directly influence cell growth (**Figure 3**) [74,75,78].

Specifically, c-MYC enhances glutaminolysis by regulating not only glutaminases, [75] but also the glutamine transporters ASCT2 and SN2, which contributes to glutamine addiction in cancer cells [77] .

In response to Rho signaling, c-JUN directly binds to the GLS promoter, thereby increasing its expression and leading to an overall metabolic reprogramming[79].

Furthermore, mTOR upregulates c-MYC translation, indirectly affecting GLS expression. This occurs because c-MYC regulates GLS in a mechanism that involves the inhibition of miRNA targeting GLS's mRNA [75]. ErbB2 has also shown to increase GLS expression through an NF-κB signaling-dependent mechanism [80] .

Besides, RhoC-NF-κB signaling pathway positively impacts GAC enzymatic activity, likely through a phosphorylation.[81] It has been demonstrated that cellular KGA activity is stimulated by EGF, and that KGA associates with all three kinase components of the Raf-1/Mek2/Erk signaling module [82] .

Nevertheless, GLS undergoes several post-translational modifications, including phosphorylation, succinylation, ubiquitinylation and acetylation which can modulate its activity. [83] In particular, phosphorylation of GAC is a crucial and responsible for the increased GLS activity in lung tumor tissues and cancer cells. [84]

GAC activity can be modified by phosphorylation at specific regions, influenced by different signaling pathways:

- Phosphorylation at Ser314: this is mediated by the oncogenic protein RhoC, and regulated by protein kinase Cε (PKCε)[84], resulting in increased in GAC levels.
- Phosphorylation at Ser95 (located at the N-terminal region of GLS): this leads to decreased GLS activity.[85]

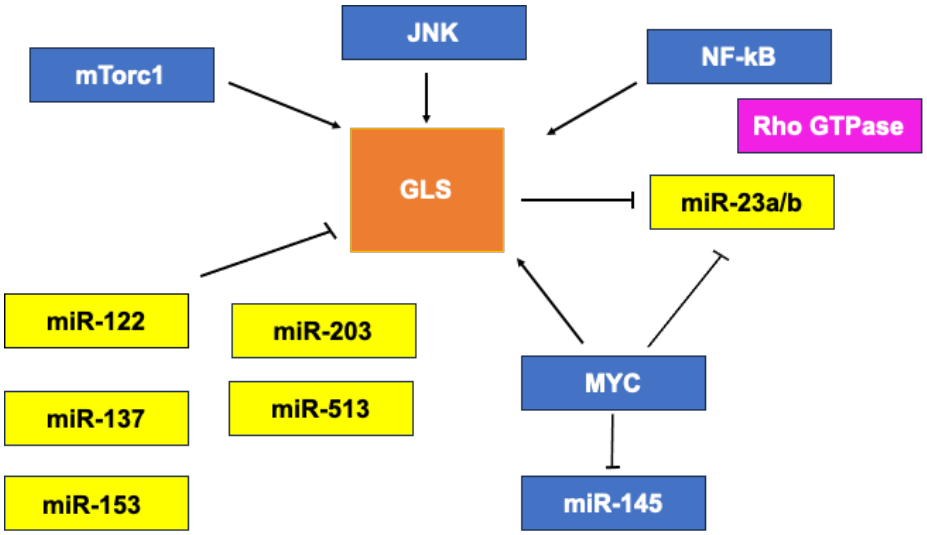


**Figure 3** ***GLS network.*** *The GLS isoforms exhibit oncogenic properties and are upregulated by various regulatory pathways such as mammalian target of rapamycin complex 1 (mTORC1), c-Jun N-terminal kinase (JNK), nuclear factor kappa-B (NF-κB), and MYC, facilitated by microRNAs (miR-23a/b). Importantly, the oncoprotein MYC can be targeted by miR-145. Additional microRNAs that downregulate GLS include miR-122, miR-137, miR-153, miR-203, and miR-513. Color codes are defined as follows: blue = transcription factors and regulatory; orange = glutaminase isoenzymes; pink = GTPases; yellow = miRs. Image modified from Matés et al., 2020.* [86]

Conversely, GLS2 exhibits tumor-suppressive features, regulated by p53[76,87–89]

Additionally, GLS2 variants show markedly increased expression in well-differentiated tumor cells. This increased expression is associated with significantly prolonged survival time. [72,76] In hepatocellular carcinoma regulation of GLS2-Rac-p53 pathway inhibits the migration, invasion, and metastasis of cancer cells. [72,90]

In astrocytoma GLS plays a key role in tumorigenesis and progression, whereas GLS2 acts as a tumor suppressor, especially in aggressive GBM subtypes. [91]

High expression of GAC is observed in all grades of astrocytoma with a gradual increase corresponding to malignancy. Indeed, a progressive activation of glutaminolysis is observed from low-grade astrocytoma to GBM and influenced by the c-Myc oncogene through miRNA mechanisms.[92,93]

Although cytosolic GLS (KGA) is more highly expressed in more malignant astrocytoma, it is less suitable for therapeutic targeting due to its elevated expression in normal tissue as well. [91] Additionally, GLS expression increases under hypoxic conditions, and its higher expression in GBM corroborates previous findings [91].

Studies on IDH mutation showed significantly reduced levels of GLN and GLU, suggesting enhanced replenishment of α–KG through glutaminolysis. As a result, wild-type (wt) gliomas exhibit high intracellular levels of GLU, which is released via the

GLN/cysteine antiporter System XC in exchange for cysteine. GSH is considered a potent antioxidant and a key factor responsible for treatment resistance in gliomas and other neoplastic cells [94,95].

The increase of GLS activity is linked also to the upregulation of GLN metabolism also in various tumors, which correlates with poor survival outcome [96].

This phenomenon underscores a hallmark of cancer: the ability of reprogram cellular metabolism to meet the high energy demands necessary for continuous proliferation and survival, mentioned in the previous paragraph as Warburg effect [98 99–101].

It is crucial to note that cancer cells can develop a dependence on GLN relying heavily on it to sustain high rates of proliferation even under conditions of hypoxia and glucose deprivation.[98–100] *In vitro* studies demonstrate that certain tumor cells cannot survive without an external supply of GLN [98,101].

Recent research further indicates that GLN promotes cancer progression not only through its metabolic role, but also by acting as a signaling molecule that activates the transcription factor STAT3. This activation is crucial for the proliferative effects of glutamine on cancer cells.[102]

Due to enhanced GLN metabolism and the high proliferation rate, cancer cells produce increased levels of reactive oxygen species (ROS). Therefore, maintaining redox homeostasis is crucial in cancer, requiring a defense mechanism to prevent apoptosis.[103] GLN helps maintain redox balance through several mechanisms, including the use of metabolites from the TCA cycle as precursors for the reducing agent NADPH.

Furthermore, intracellular GLU exchange via the SLC7A11 transporter facilitates cystine uptake, which is subsequently reduced to cysteine, the rate-limiting precursor for GSH biosynthesis [104] .

Both NADPH and GSH are essential regulators of cellular redox status [103,105].

Finally, there is a crosstalk between GLN/GLS and mTOR pathway. mTORC1, a key kinase regulating cell growth and proliferation, relies on glutamine-derived α-KG for GTP loading of RagB and subsequent activation.[106] In turn, mTORC1 positively regulates GLS by enhancing Myc translation efficiency[107] .Furthermore, GLN efflux through SLC7A5 is linked with leucine uptake, a potent activator of mTORC1[108].

Both GLS and mTOR proteins have emerged as therapeutic targets capable of impairing GBM tumorigenicity and metabolic plasticity.

### 2.9. GLS as a target for cancer therapy

The reliance of cancer cells on GLN highlights targeting glutaminolysis as a promising therapeutic strategy.

Recent clinical approaches have focused on inhibiting GLS, the key enzyme in GLN metabolism for tumor growth.

Chemical inhibitors have proven effectiveness in reducing cancer cell proliferation both *in vitro* and *in vivo*. Early GLS inhibitors used in preclinical studies were non-selective and associated with undesirable effects. For instance, 6-diazo-5-oxo-L-norleucine, which structurally resembles GLN and has reactive chemical properties, prompted the development of more specific compounds [109].

Two notable inhibitors, BPTES and dibenzophenanthridine-968, have been identified.

BPTES selectively inhibits GLS more than GLS2 in various cancers forming an inactive tetramer complex with GLS [110], avoiding competition with GLN at the catalytic site.[79,109,111]

This inhibitor has shown efficacy in glioma cells, reducing GLU and α-KG levels, thereby slowing tumor growth [111]. Although BPTES selectively inhibits GLS over GLS2, it has been reported to have limitations in pharmacological application, owing to its poor metabolic stability, low solubility, and moderate potency[112].

Like BPTES, dibenzophenanthridine-968 is an allosteric inhibitor of GLS and inhibits the activity of KGA and GAC[113] .

Mouse xenograft model studies have demonstrated its antitumor activity in lymphoma, breast cancer, ovarian cancer, and glioblastoma cells [76,79,114].

Recently, a derivative of BPTES, known as CB-839, has been developed (**Figure 4**). Like BPTES, CB-839 belongs to the benzo[a]phenanthridinone family [98] and inhibits GLS by targeting its allosteric site, stabilizing the enzyme in an inactive tetrameric state[111,115].

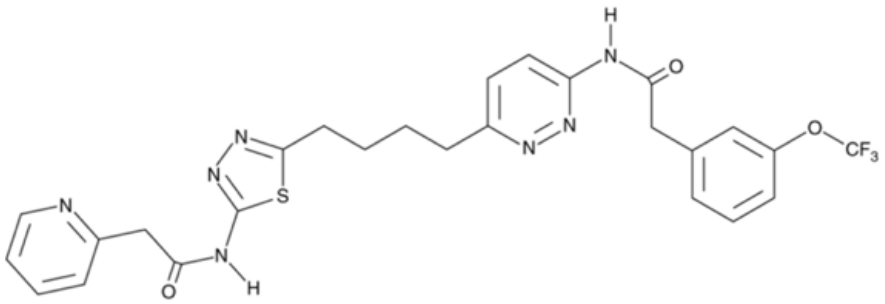


**Figure 4** ***Molecular structure of CB-839.*** *CB-839, as known with its commercial name Telaglenastat is a potent, selective, and orally bioavailable glutaminase inhibitor (from* [https://www.selleckchem.com/products/cb-839.html](https://www.selleckchem.com/products/cb-839.html))

The inhibition of CB-839 regulates the enzymatic activity of KGA and predominantly the GAC splice variant isoenzyme [79,116].

CB-839 has more potency compared BPTES, requiring lower concentrations to achieve therapeutic effects [79,109,110].

*In vivo* studies with this small molecule have shown that the brain accumulation of CB-839 is significally hindered, most likely due to the challenge of crossing the BBB[117]. Therefore, the general bioavailability of the CB-839 into the tumor sites, as oral administration of the compound required severely high dosages to achieve therapy efficacy. New strategies to ensure more effective penetration of this promising drug candidate to tumor cells are urgently required, including the use of gold nanoparticles (Au NPs). The use of nanomaterial could enhance permeation and retention (EPR) effect in tumors and could successfully transverse the cell membrane barrier of the GBM cells[118,119].

Preclinical models have shown that CB-839 causes substantial growth inhibition in certain breast cancer (BC) subtypes, particularly triple-negative breast cancer (TNBC) cells, which are more sensitive to this inhibitor than luminal A/estrogen receptor-positive cells due to their higher GLN dependence and enhanced GLN utilization. [116] Treatment with CB-839 has demonstrated promising results, halving TNBC growth in mouse models injected with tumor cells[116,120] .

The ongoing Phase I and II clinical trials are summarized in table (**Table 2**) below.

**Table 2** Clinical trials using the GLS inhibitor CB-839[121]

| Cancer type | Clinical trial phase | Clinical trial number |
|---|---|---|
| Renal cell carcinoma | Phase II | NCT03428217 |
| Melanoma | Phase I/II | NCT02771626 |
| NSCLC | Phase I/II | NCT02771626 |
| Colorectal | Phase I/II | NCT02861300 |
| Myelodysplastic syndrome | Phase I/II | NCT02071927 |
| Breast (TNBC) | Phase I/II | NCT02071862 |

NSCLC, Non-small-cell lung carcinoma; TNBC, Triple-negative breast cancer.*Source:* National Cancer Institute.

### 2.10. Crosstalk between epigenetics and metabolism

Epigenetic modifications play a pivotal role in regulating transcriptional processes and contribute significantly to metabolic reprogramming[122]. Concurrently, metabolites derived from metabolic pathways within the tumor microenvironment serve as substrates for histone modifications and DNA methylations[123] .

Advancements in understanding the bidirectional communication between epigenetics and metabolism are crucial for exploring the mechanisms underlying carcinogenesis and metastasis. These insights provide strategic avenues for cancer prevention and therapy. Metabolic disturbances arise from the abnormal accumulation of metabolites, known as oncometabolites. Among the most studied are succinate, fumarate, and 2-hydroxyglutarate (2-HG), which notably inhibit α-ketoglutarate (α-KG)-dependent dioxygenases. The accumulation of 2-HG is frequently associated with IDH1 mutations found in glioblastoma (GBM) and other cancers[124–126] .

2-HG primarily functions by reshaping the DNA methylome, particularly impacting CpG island methylation patterns that affect Jumonji C domain (JmjC)-containing histone lysine demethylases (KDMs). Additionally, succinate and fumarate remodel DNA through inhibition of KDMs and 5-methylcytosine (5mC) hydroxylases, influencing gene expression crucial for cellular differentiation and acquisition of malignant traits.[127–129]

Histone acetyltransferases (HATs) add acetyl groups to chromatin histone tails, while histone deacetylases (HDACs) remove them. Acetyl-CoA, derived from glycolysis, pyruvate, fatty acid oxidation, acetate, and amino acids, plays a pivotal role in mitochondrial function and gene expression regulation [130]

Histone methyltransferases (HMTs) and histone demethylases (HDMs) utilize S-adenosyl methionine (SAM) for methyl group transfer. SAM is generated through the coupling of folate and methionine cycles in the cytosol, supported by one-carbon metabolism in mitochondria. Methylation of specific residues such as lysine 4, 36, and 79 on histone H3 (H3K4, H3K36, H3K79) activates gene expression, while methylation of H3K9, H3K27, and H4K20 represses gene expression. [131]

DNA methylation occurs in CpG islands, specific regions of DNA rich in CpG sites where cytosine and guanine are linked by a phosphodiester bond. The activity of DNMT1, DNMT3A, and DNMT3B, key DNA methyltransferases, depends on SAM availability.[132]

This intricate interplay between epigenetics and metabolism underscores the complexity of devising effective therapeutic strategies, suggesting the necessity of a multifaceted approach.

### 2.10.1. Lysine specific demethylase 1 (LSD1)

#### 2.10.1.1. LSD1: molecular structure and its role in GBM

The lysine-specific histone demethylase 1 (LSD1), also called KDM1A, acts as an oxidase enzyme that modifies histone proteins by removing specific methyl groups from lysine residues. It targets and alters methylation marks at H3K4 and H3K9, which are pivotal for controlling gene activity[60].

- Structurally, LSD1 features three distinct parts[61]:
  - the SWIRM domain, crucial for binding to its substrate and guiding its localization within the cell.
  - the AOL domain, divided into two sections by the TOWER domain:
    - The right AOL forms the functional core where LSD1 interacts with its substrate directly.
    - The left AOL binds FAD, an essential co-factor that enables LSD1's catalytic activity.
  - the TOWER domain extends outward and serves multiple roles:
    - It interacts with proteins that stabilize LSD1, shielding it from degradation.
    - It facilitates LSD1's engagement with chromatin, helping to open DNA structures and enabling LSD1 to perform its demethylation function effectively

Overall, LSD1 enzymatic role is crucial for regulating gene expression through epigenetic mechanisms. Its activity influences essential biological processes such as embryonic differentiation (where its absence is lethal), neurogenesis in neural stem cells, and the maintenance of stem cell populations [62,63].

This enzyme's pivotal role in normal physiological settings underscores its significance[63]. However, dysregulation of LSD1 is implicated in various pathological conditions, including cancer development. In tumors, LSD1 is frequently overexpressed, and studies have established a clear association between increased LSD1 levels and tumor formation. [64–66].

In GBM, LSD1 plays a critical role in maintaining TICs. Prominent levels of LSD1 in GBM correlate with poorer prognosis for patients. Researchers are exploring ways to target LSD1 in GBM TICs through methods such as genetic silencing or pharmacological inhibition. These approaches aim to suppress LSD1's activity, potentially offering new therapeutic strategies against this aggressive form of brain cancer.

In our laboratory, we used primary TICs from GBM to evaluate the impact of a new, irreversible LSD1 inhibitor called DDP_38003 (hereafter referred to as LSD1i), developed at the European Institute of Oncology.

This inhibitor has shown high specificity and the ability to penetrate the BBB effectively.[67]

Previous studies have demonstrated that LSD1 inhibition halts cell growth, induces apoptotic cell death, and reduces stem-like characteristics *in vitro*[14,16].

Moreover, *in vivo* studies have indicated that LSD1 inhibition reduces the ability of tumors to form and slows down tumor growth[68,69].

These findings highlight the potential of LSD1 inhibitors as promising therapeutics against cancers, including GBM, driven by LSD1's tumor-promoting activity.

The development of selective and brain-penetrant LSD1 inhibitors like LSD1i represents a significant advancement in this field, with potential therapeutic benefits comparable to those observed in mouse models of leukemia[70].

# 3. AIMS AND PRELIMINARY RESULTS

We have recently shown in the context of GBM that pharmacological targeting with LSD1 inhibitor (LSD1i) can counteract TIC characteristics and reduce overall tumor aggressiveness. Our research indicates that LSD1 has non-enzymatic role, in activating the integrated stress response (ISR), a mechanism that helps cells adapt to various tumor-related stresses regulated by Activating Transcription Factor 4 (ATF4). LSD1 inhibition interferes with ATF4 and its related genes, delaying ISR activation and leading to cell death. However, LSD1i is only effective in a subset of GBM-TICs, named LSD1i-sensitive (hereafter LSD1i$^{sens}$). We have identified a subset of TICs resistant to LSD1i (hereafter LSD1i$^{res}$).

Recently, we focused on characterizing this patient-derived TICs cohort that displayed resistance to LSD1i and explored the molecular mechanisms by which GBM-TICs bypass LSD1i efficacy.

Our hypothesis is that these drug-resistant cells are able to survive under metabolic changes such as those in a GBM energy-deprived environment. Our recent results suggest that when these cells are stressed by nutrient shortages or ER stress, they can maintain energy balance through the activation of ATF4 signaling pathway.

Since we demonstrated that metabolic plasticity protects LSD1i-resistant TICs from stress and supports their growth, we performed a synthetic lethal shRNA screening exploiting a barcoded library of shRNAs against essential metabolic genes (*unpublished data*) (**Figure 5**).

LSD1i$^{Res}$ TICs were exposed to either LSD1i (2.5-5μM) or a vehicle for up to eight weeks in culture. After sequencing the barcoded DNA from surviving cells, we identified genes that were not counterselected in the control condition, but were depleted only upon LSD1i treatment consistently across replicates.

This process led to the identification of 14 genes that likely contribute to LSD1i resistance (**Figure 5a**). The different expression of mRNA levels of these 14 selected metabolic genes in patients with GBM has been confirmed by “The Cancer Genome Atlas” dataset (TCGA) analysis (**Figure 5b**).

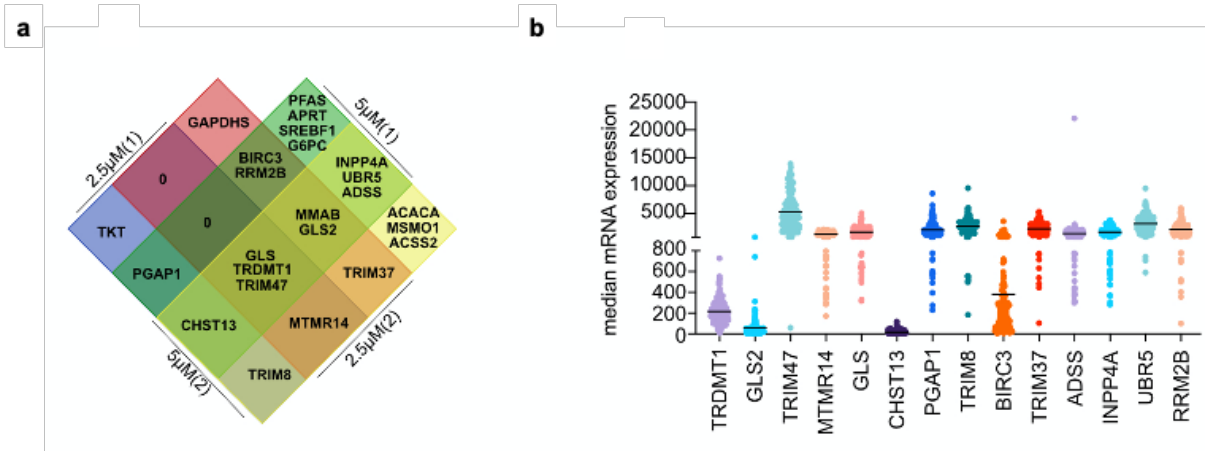


**Figure 5** ***In vitro synthetic lethal shRNA screening***. ***a.*** *Venn diagram shows genes in common among the replicates.* ***b.*** *mRNA expression levels of the selected metabolic genes from TCGA dataset* (*unpublished data*).

Hence, our attention is focused on GLS which underpins glutaminolysis, a hallmark of cancer metabolism.

The thesis aims to analyze the role of GLS using neurospheres as in vitro models, with the goal of defining and validating new therapeutic strategies for targeting GBM TICs. Specifically, we propose a combination approach involving LSD1 inhibitor with compounds that target glutamine metabolism pathways. To this end, we focused on characterizing resistant TICs in terms of proliferation and analyzing the metabolic differences between sensitive and resistant TICs to understand their intrinsic vulnerabilities.

# 4. MATERIALS AND METHODS

## 4.1. Cell Culture

GBM-TICs were isolated from human-GBM surgical specimen[211] collected from consenting patients in in the Department of Neurosurgery at Neurological Institute “C. Besta” (Milan, Italy) under “C. Besta research ethics committee approval”, were already available in the laboratory. GBM-TICs used for experiments are named: GBM#7, GBM#22, GBM#23, GBM#25. As described in the previous section, GBM-TICs are distinguished into two main subsets: LSD1i$^{sens}$ (specifically GBM#7, GBM#22); LSD1i$^{Res}$ (specifically GBM#23, GBM#25).

GBM-TICs were retrieved by enzymatic digestion of the tumor with papain 2 mg/mL (Worthington Biochemical) at 37°C followed by mechanical disruption to obtain a single cells suspension. To remove red blood cells, 3-5 minutes of ACK (Ammonium-Chloride-Potassium) Lysis Buffer incubation was performed.

GBM primary TICs were cultured as spheroid aggregates in serum-free medium DMEM-F12 1:1 (Dulbecco’s Modified Eagle Medium-Ham’s F12 Nutrient Mixture) supplemented with B27 supplement (Life Technologies, Paisley, United Kingdom), 20 ng/ml EGF and 10ng/ml b-FGF (Pepro Tech, Rocky Hill, NJ) and maintained at 37°C in a 5% $CO_2$ humidified incubator. TICs were passaged by mechanical dissociation when the sphere reached approximately 300-500 microns in diameter. Briefly, the cell suspension was transferred to a sterile tube and centrifuged at RT for 5 minutes at 400-600 rpm depending on the spheres’ dimensions. The supernatant was carefully removed and pelleted spheres were washed with PBS 1X and dissociated mechanically to obtain a single cell suspension. Single cells were centrifuged at 1200rpm at RT for 5 minutes and the pellet was resuspended and plated in complete medium.

## 4.2. Chemicals

Telaglenastat (CB-839) ($C_{26}H_{24}F_3N_7O_3S$) was provided by Selleckchem. CB-839 was administered at concentrations between 1 and 50 μM as specified for individual experiments. LSD1 inhibitor (LSD1i, DDP_38003) was synthesized by the Experimental Therapeutic Unit at the IFOM-IEO Campus. As a vehicle control for both CB-839 and LSD1 inhibition, GBM TICs were grown in complete medium supplemented with 0,03% DMSO. All compounds were administered once at the time of plating.

### 4.3. Proliferation

GBM TICs were plated in technical triplicate in a 24 well plate (50.000 cells/well for GBM#22 and GBM#7, 100.000 cells/well for GBM#23 and GBM#25). Cells were counted with Invitrogen Countess 3 Automated Cell at the indicated time points. Cell growth of scrambled and shGLS#6A of GBM-TICs was assessed with the same approach and the number of cells was normalized to the number of cells plated (day 0) or scrambled condition.

### 4.4. Apoptosis Assay

Caspase 3/7 activity was measured with Caspase-Glo assay kit (Promega) after CB-839 [10 μM] treatment. 10.000 GBM-TICs were seeded as single cells in 100μL in a white 96 well plate. At the indicated time point, 100μl of Caspase-Glo reagent was added to each well and the plate was gently mixed with a plate shaker for 30 seconds. After 30 minutes of room temperature incubation in the dark, caspase activity was measured in a plate-reading luminometer (GloMax) at timepoint of 24, 48 and 72h.

### 4.5. GBM-TICs Lentiviral Infection

The 3$^{rd}$ generation of lentivirus is produced using transfer vector, pRSV Rev, pMDLG/RRE, VSVG envelope plasmid in 293T cells. Supernatants were collected and ultracentrifuged at 22000 rpm for 2 hours. Concentrated virus was used to infect GBM-TICs (GBM#22,#7,#23,#25) and after 48 hours, cells were selected with puromycin. Cells were kept in culture up to six weeks and splitted once a week.

shRNA oligonucleotides targeting GLS was chosen from the library, based on their ranking in screening analysis and cloned into pRSI17-U6-(sh)-UbiC-GFP-2A- Puro linearized expressing vector, according to the manufacturer's instructions (Cellecta). A scrambled constitutive lentiviral plasmid was used as control.

### 4.6. Western Blot

GBM TICs were seeded in a 6well plate (1e06 cells/well) and collected at the indicated timepoint by centrifugation at 1200rpm for 5' at +4ºC with one wash with PBS 1X. Cells were lysed in RIPA buffer (50 mM Tris-HCl buffer (pH=8), 10 mM $CaCl_2$, 5mM EGTA (pH 8), 250 mM NaCl, Glycerol 10%, triton-x100 1%) supplemented with a cocktail of proteinase inhibitors (50 mM NAF, 10 mM NAPP, 10mM NaOrtoV, PMSF (0.1mg/ml), Leupeptin 10 μM, Aprotinin 10 μM) . Protein lysates were incubated for 20' on ice and then centrifuged at 13,000 rpm for 15' at +4°C to separate the cellular debris and nuclei from the soluble protein fraction. The supernatant was carefully transferred to a fresh

microcentrifuge tube and stored at -20°C if not used immediately. Proteins were quantified by Bradford assay following the manufacturer instructions. 10 µg of proteins was mixed with 5X Laemmli buffer containing 50nM DTT and $ddH_2O$, then denatured by heating at 95°C for 5 minutes. Proteins were separated by SDS-polyacrylamide gel electrophoresis (SDS-PAGE). Gels were prepared with 10% Bis/Acrylamide, 10% APS and 0,001% TEMED. The gel was run at a constant voltage until the dye front reached the bottom. Proteins were transferred to a nitrocellulose membrane of 0.2 µm pore size using a wet or semi-dry transfer system. The membrane was incubated in a blocking solution with 5% bovine serum albumin in Tris-Buffered Saline and Tween 20 (TBS-T [50mM Tris, 150 mM NaCl, 0.05% Tween 20]). Membranes were incubated overnight at 4°C with primary antibodies against GLS (abcam#156876,1:1000), Cleaved Parp (Cell Signaling #5625, 1:1000), Parp (Cell Signaling #8007,1:1000), tubulin (sigma T9026,1:1000), vinculin (sigma v9131,1:1000).

Antibody binding was assessed by horseradish peroxidase (HRP) conjugated secondary antibody (1:5000, Sigma Aldrich). Images were acquired on a ChemiDoc XRS instrument (Biorad). Densitometric quantification of band intensity was carried out using the band analysis tools of ImageLab software version 4.1 (Bio-Rad). Intensity of bands from the protein of interest is normalized to the intensity of the housekeeping (HK) bands, and is expressed as fold change relative to the untreated sample.

### 4.7. Real Time-qPCR

RNA was extracted from GBM-TICs using the Quick-RNA Miniprep (Zymo Research) as indicated in the manufacturer's protocol. RNA quantification was performed by using the NanoDrop spectrophotometer.

cDNA was synthesized with the High-Capacity Reverse Transcription Kit (Applied Biosystems). Gene expression was assessed by RT-qPCR by QuantStudio (applied biosystems) using Fast SYBR Green (Applied Biosystems). Threshold cycle (Ct) values for each gene were normalized to the housekeeping (HK) genes (TBP,18s, RPL0, GADPH) expression. Relative expression was determined by the $2^{-\Delta\Delta}$ where ΔCt was calculated as follows: ΔCt= Ct (gene of interest) – Ct (HK)).

Primer sequences are as follows:

| | FORWARD | REVERSE |
|---|---|---|
| 18s | CGCCGCTAGAGGTCAAATTC | CTTTCGCTCTGGTCCGTCTT |
| GAC | AGGTGGTGATCAAAGGCATTC | GAGATGTCCTCATTTGACTCAGGT |
| GAPDH | AGCCACATCGCTCAGACAC | GCCCAATACGACCAAATCC |
| GLS | TGGTGGCCTCAGGTGAAAATA | GGGATCAGACGTTCGCAATC |
| KGA | CTGGAAGCCTGCAAAGTAAAC | TGAGGTGTGTACTGGACTTGG |
| RPL0 | TTCATTGTGGGAGCAGAC | CAGCAGTTTCTCCAGAGC |
| TBP | TGCACAGGAGCCAAGAGTGA | CACATCACAGCTCCCCACCA |

### 4.8. Glutaminase (GLS) Activity Assay Kit

GLS Activity Assay Kit (ab284547) is a plate-based fluorometric assay. $1x10^6$ cells were homogenized in GLS buffer, performing lysis on ice for 10 minutes followed by centrifugation at 10,000xg for 15 minutes at 4ºC. Supernatants were collected and protein quantification was estimated using Bradford assay. Glutamate standard curve was generated to estimate amount of glutamate formed as manufactures. Glutaminase activity may be calculated using glutamate formed, starting from GLN conversion in glutamate and ammonia. Glutamate in the presence of a developer and enzyme mix converts a non-fluorescent probe to a fluorescent product via an enzymatic reaction**.** The fluorescence signal (Ex/Em = 535/587 nm) was recorded on kinetic mode at 37°C set to every 30 second by PHERAstar. The GLS activity was calculated as a rate of nmol of GLU formed and sample protein content added to well (mg).

### 4.9. Statistical analysis

Statistical analysis was performed using Statistical Prism 8.0 software. Results are the average from 3 technical replicates. Data plotted with error bars represent Mean ± Standard Deviation. Two-way ANOVA (followed by Sidak's multiple comparison test) and unpaired Student's t-test were performed to test the significance of differences observed between experimental groups. Differences were considered "statistically significant" when $p<0.0001$(****); $p<0,0003$ (***); $p<0,0033$ (**); $p<0,0205$ (*).

# 5. RESULTS

## 5.1. GLS expression in patient-derived GBM-TICs

Since our preliminary data defined GLS as a driver of LSD1i resistance, we first examined the level of GLS protein expression in both LSD1i$^{sens}$ and LSD1i$^{res}$ GBM TICs. Using an anti-GLS antibody capable of detecting both GLS isoforms (KGA and GAC) by Western Blot, we were able to distinguish the presence of both GLS isoforms (KGA and GAC) in LSD1i$^{res}$ and LSD1i$^{sens}$ TICs as indicated by red arrows in the **Figure 6**. Interestingly, we observed a differential expression of the two GLS isoforms in equal manner in both resistant and sensible cells (**Figure 6a**). Compared to the KGA expression level, the GAC isoform (55kDa) is more prevalent in the LSD1i$^{res}$ and LSD1i$^{sens}$ TICs examined (**Figure 6b**).

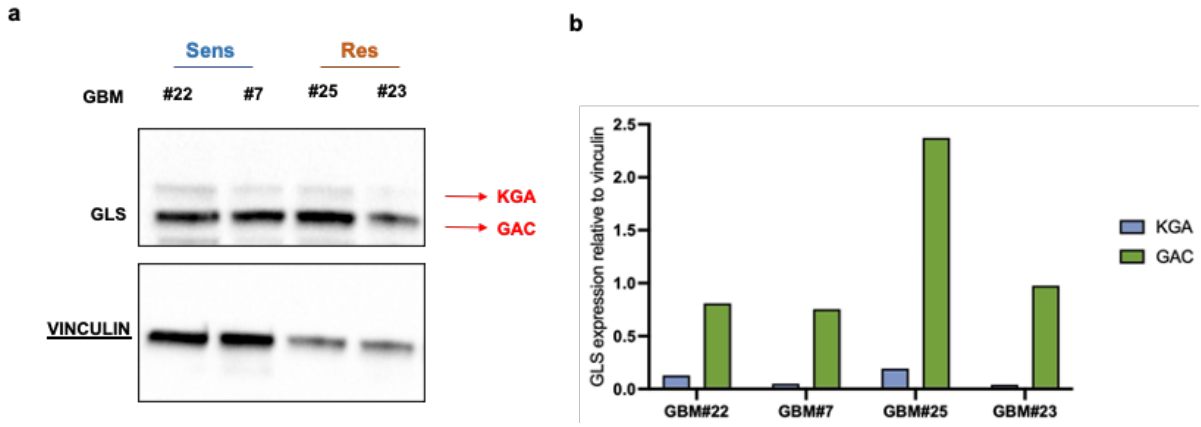


**Figure 6** ***GLS expression in LSD1i$^{sens}$ and LSD1i$^{res}$ GBM TICs***. ***a***. *Western blot of GLS in GBM#22 #7# #25 #23.* ***b.*** *Quantification of GLS expression relative to the two isoforms of GLS (KGA and GAC) in GBM#22 #7# #25 #23. Data were normalized on Vinculin.*

We further performed qPCR analysis on both GBM TICs cohorts to validate the differential expression of the two GLS isoforms, using primers to detect total GLS and its isoforms (KGA and GAC).

The results show that total GLS is expressed in all GBM TICs (**Figure 7**).

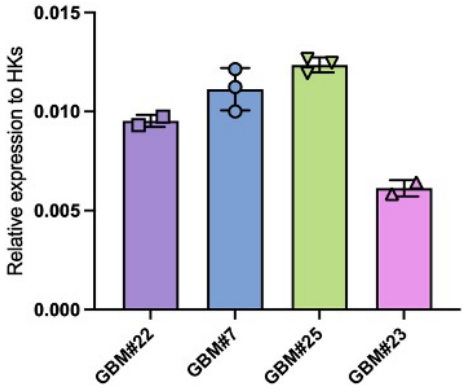


**Figure 7** ***Relative mRNA expression of GLS in LSD1i$^{sens}$ and LSD1i$^{res}$ GBM-TICs by qPCR.*** *Results show one experiment, expressed as mean +/- SD (n=3 technical replicates for each GBM-TIC). Data were normalized on the geometric mean expression of four housekeeping genes (TBP, RPLPO, GAPDH, 18S).*

Even in transcriptional analysis, GAC is expressed more than KGA in all TIC cohorts (**Figure 8**).

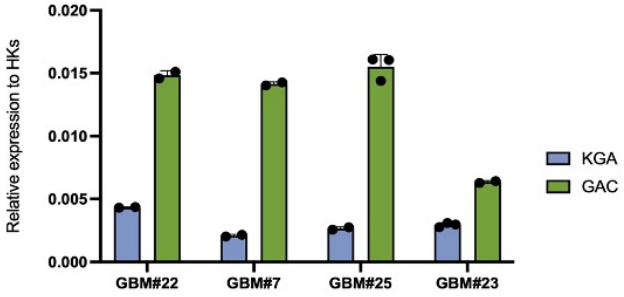


**Figure 8** ***Relative mRNA expression of KGA and GAC in LSD1i$^{sens}$ and LSD1i$^{res}$ GBM-TICs by qPCR****. Results show one experiment, expressed as mean +/- SD (n=3 technical replicates for each GBM-TIC). Data were normalized on the geometric mean expression of four housekeeping genes (TBP, RPLPO, GAPDH, 18S).*

### 5.2. Glutamine dependency of LSD1i$^{sens}$ and LSD1i $^{res}$ TICs

Next, we assessed the dependency of GBM TIC samples on glutamine by seeding GBM TICs in low-glutamine-condition medium (0,5 mM GLN) and in standard-glutamine-condition medium (2 mM GLN). We evaluated the effect on cell growth after 5 days (**Figure 9**).

Low glutamine-levels did not affect cell growth in LSD1i$^{sens}$ TICs (GBM#22 and GBM#7) 5 days after cell seeding. In contrast, LSD1i$^{res}$ TICs (GBM#23 and GBM#25) showed a relevant decrease in cell number under the same conditions.

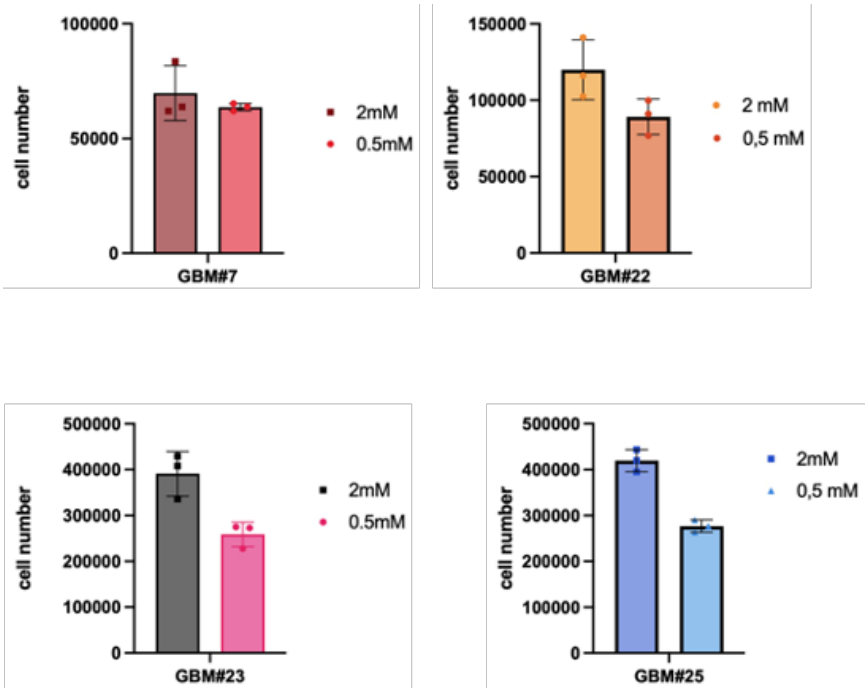


**Figure 9** ***Cell growth of LSD1i$^{sens}$ and LSD1i$^{res}$ GBM-TICs in low and standard GLN conditions****. GBM#7 #22 #23 #25 were seeded in 0.5 mM GLN (low GLN) and 2 mM GLN (standard GLN) in culture medium. The cell viability was assessed after 5 days. Results show one experiment, expressed as mean +/- SD (n=3 technical replicates for each TIC).*

### 5.3. GLS silencing elicits different response in LSD1i$^{sens}$ and LSD1i $^{res}$ TICs

Parallel to pharmacological GLS targeting, we silenced the GLS gene with shRNA in LSD1i$^{res}$ and LSD1i$^{sens}$ TICs and a scrambled constitutive lentiviral plasmid was used as control. We tested the efficiency of GLS silencing in shGLS compared to scrambled cells by Western Blot (**Figure 10**).

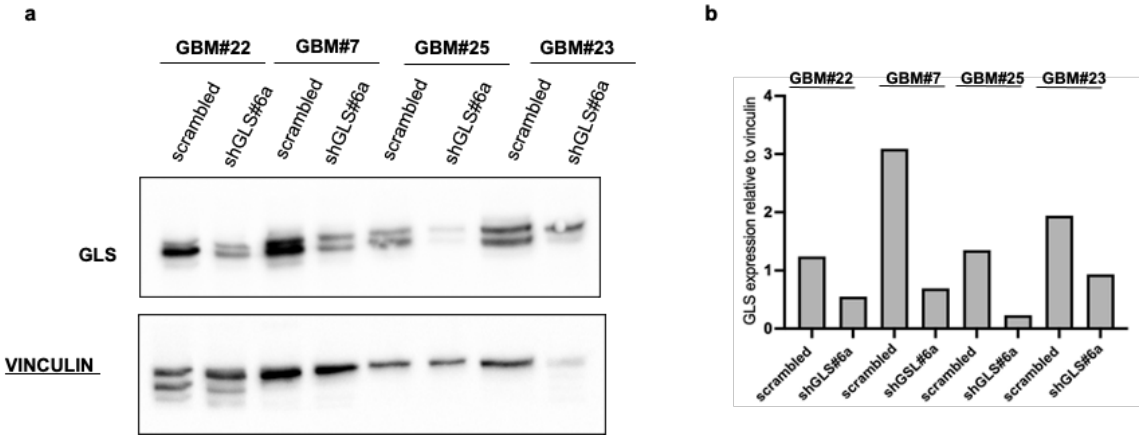


**Figure 10** ***GLS silencing in LSD1i$^{sens}$ and LSD1i$^{res}$ GBM-TICs a.*** *Western Blot of GLS level expression in scrambled and shGLS conditions in GBM#22 #7 #25 #23.* ***b.*** *Quantification of GLS protein expression. Data were normalized on Vinculin*

Quantitative analysis of GLS protein expression indicates that GLS protein levels were approximately 70% lower in shGLS cells compared to scrambled GLS cells (**Figure 10b**). This decrease in signal was quantified as percentage of shGLS relative to scrambled condition and detailed in **Table 3.**

**Table 3**

| | GLS signal reduction in shGLS#6a cells (%) |
|---|---|
| GBM#22 | 55,7 |
| GBM#7 | 77,7 |
| GBM#25 | 82,8 |
| GBM#23 | 52,0 |

We further validated GLS depletion in LSD1i$^{res}$ TICs (GBM#23) using GLS activity assay. As shown in **Figure 11**, GLS activity in shGLS cells. decreased by approximately of 25%, measured as the amount of glutamate per protein mg.

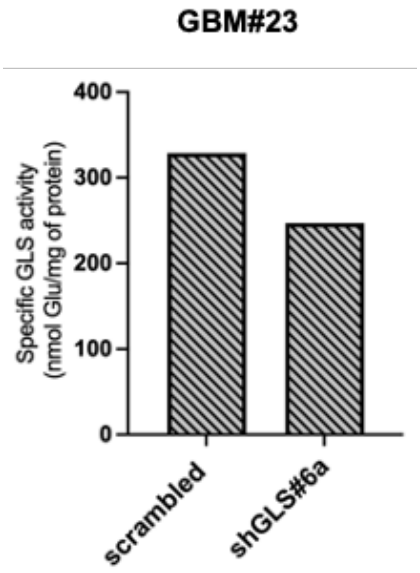


**Figure 11** ***GLS activity in scrambled and shGLS#6a GBM#23.*** *Results are expressed as nmol of produced glutamate per milligram of protein added. The amount of formed glutamate is estimated using the standard curve, according to kit protocol.*

To evaluate the effect of GLS silencing in both TIC cohorts, we assessed the cell growth of shGLS#6a TICs and scrambled TICs at 3, 5, 7 days after plating (day 0) (**Figure 12**). In the sensitive LSD1i cell line (GBM#22), both scrambled and shGLS#6a proliferate similarly with no significant differences over time (**Figure 12a**). Conversely, in LSD1i$^{res}$ TICs (GBM#23), shGLS#6a cells exhibit slower growth compared to the scrambled cells.

Specifically, shGLS#6a LSD1i$^{res}$ cells proliferate between day 0 and 5, but, from day 5 to day 7, the number of cells remain constant (**Figure 12b**).

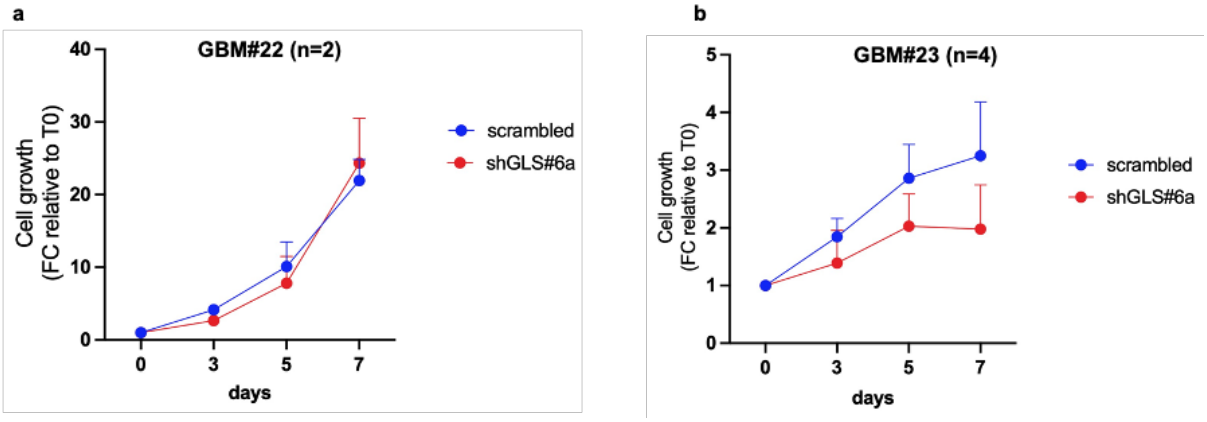


**Figure 12** ***Cell growth upon GLS silencing in LSD1i$^{sens}$ (GBM#22) and LSD1i$^{res}$ (GBM#23) GBM-TICs.*** ***a.*** *GBM#22 curve proliferation at the time points indicated (3,5,7 days from day of cell plating). Results show 2 biological replicates, expressed as mean +/− SD.* ***b.*** *GBM#23 proliferation curve at the time points indicated (3,5,7 days from day of cell plating). Results show 4 biological replicates, expressed as mean +/− SD.*

### 5.4. GLS silencing to enhance the sensitivity of LSD1i$^{res}$ GBM-TICs to LSD1i treatment

We treated shGLS#6a and scrambled LSD1i$^{res}$ TICs (GBM#25 cells) as well as shGLS#6a and scrambled LSD1i$^{sens}$ TICs (GBM#7 cells) with increasing doses of LSD1i and evaluated cell growth after 7 days (**Figure 13**).

In the scrambled condition of LSD1i$^{sens}$ TICs treated with LSD1i, we observed a pronounced dose-dependent reduction in cell growth, consistent with previous findings from Faletti *et al.*[133]. However, the combination of GLS silencing and LSD1i treatment did not demonstrate either synergistic or additive effects on the growth of LSD1i$^{sens}$ TICs (**Figure 13a**).

In LSD1i$^{res}$ TICs (GBM#25 cells), GLS silencing significantly impacted cell proliferation. The combination of GLS silencing and LSD1i treatment did not restore sensitivity in resistant cells to LSD1 inhibitor treatment. (**Figure 13b**).

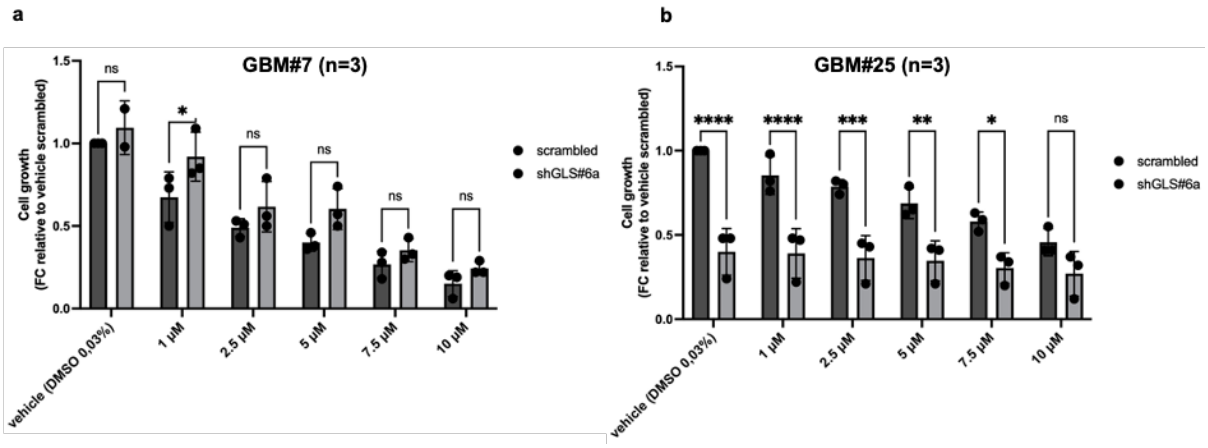


**Figure 13** ***Cell growth of scrambled and shGLS#6a LSD1i$^{sens}$ (GBM#7) and LSD1i$^{res}$ (GBM#25) GBM TICs upon LSD1i treatment***. ***a.*** *scrambled and shGLS#6a GBM#7 proliferation after treatment with different LSD1i doses [1-2,5-5-7,5-10µM]. Cells viability was evaluated after 7 days.* ***b.*** *scrambled and shGLS#6a GBM#25 proliferation after treatment with different LSD1i doses [1-2,5-5-7,5-10µM]. Cells viability was evaluated after 7 days. Results show 3 biological replicates, expressed as mean +/− SD (two-way ANOVA followed by Sidak's multiple comparison test; ****p<0.0001; ***p<0,0003;**p<0,0033;*p<0,0205).*

## 5.5. Pharmacological inhibition of GLS has antiproliferative effect in LSD1i$^{sens}$ and LSD1i$^{res}$ TICs

To assess the effect of GLS inhibition on LSD1i$^{res}$ TICs, we employed Telaglenastat (CB-839) that inhibits the catalytic activity of GLS.[134,135]

Initially , we assessed GLS activity in GBM#22 after CB-839 treatment (50 µM), using DMSO as a vehicle control. We observed a significant reduction in GLS activity, approximately 50%, with the high dose of CB-839 (**Figure 14**).

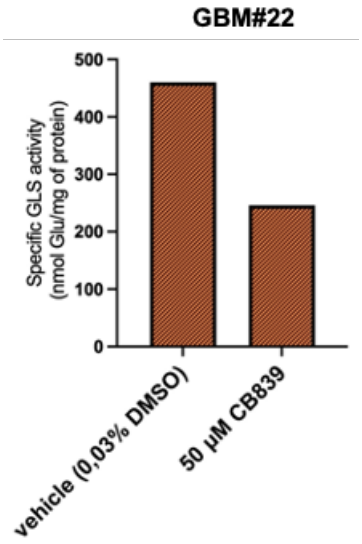


**Figure 14** ***GLS activity after CB-839 treatment in LSD1i$^{sens}$ GBM-TICs (GBM#22)****. Results are expressed as nmol of produced glutamate per milligram of protein added. The amount of formed glutamate is estimated using the standard curve, according to kit protocol. 0,03% DMSO is used as vehicle.*

We examined the effects of increasing doses of CB-839 (ranging from 1 to 50 μM) on the cell growth of LSD1i$^{sens}$ and LSD1i$^{res}$ TICs (**Figure 15**). We observed a dose-dependent response in terms of cell growth following CB-839 administration. EC50 value of CB-839 was calculated to be 10 μM in both LSD1i$^{sens}$ TICs (GBM#7 and GBM#22) and LSD1i$^{res}$ TICs (GBM#23 and GBM#25).

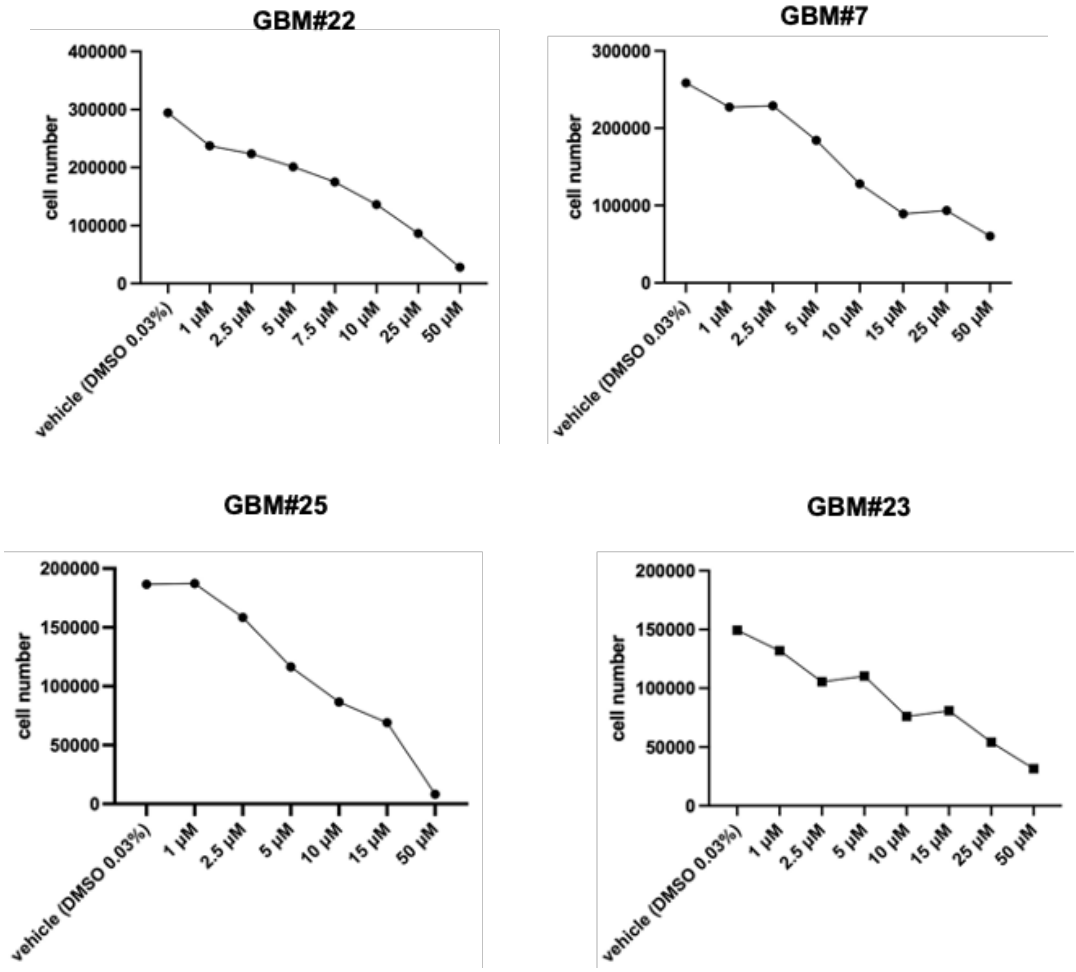


**Figure 15** ***Cell growth after treatment with different CB-839 doses in LSD1i$^{sens}$ and LSD1i$^{res}$ GBM-TICs****. GBM#7 #22 #25 #23 are treated with 1-2,5-5-10-15-25-50 μM of CB-839. Cells viability was evaluated after 72h. Results show one experiment in terms of cell number. 0,03% DMSO is used as vehicle.*

## 5.6. Pharmacological inhibition of GLS with CB-839 treatment induces apoptosis in LSD1i$^{sens}$ and LSD1i$^{res}$ GBM-TICs

Consistent with the observed decrease in GBM-TICs growth after CB-839 treatment, we investigated apoptosis activation (**Figure 16**).

At three time points (24,48,72h), we measured high caspases 3/7 activity after CB-839 treatment in LSD1i$^{sens}$ TICs (GBM#22 cells) (**Figure 16a**).

Additionally, we examined the activation of the apoptotic pathway upon GLS pharmacological inhibition in both LSD1i$^{sens}$ (GBM#22) and LSD1i$^{res}$ TICs (GBM#23). We used Western blot analysis to detect cleaved-PARP, a marker of cell-death proteases, after CB-839 treatment.

In the control condition of both GBM-TICs, cleaved-PARP exhibited minimal expression relative to total-PARP, indicating the absence of apoptosis. Following CB-839 treatment, the level of cleaved-PARP increases, suggesting that CB-839 induces apoptosis in a dose-dependent manner (**Figure 16b and d**).

To further confirm the efficacy of CB-839 treatment in the LSD1i$^{res}$ cell line (GBM#23), we measured the percentage of dead cells after 72h with increasing drug doses. The results show a gradual increase in cell death and a corresponding decrease in cell number with progressively higher doses of the inhibitor (**Figure 16c**).

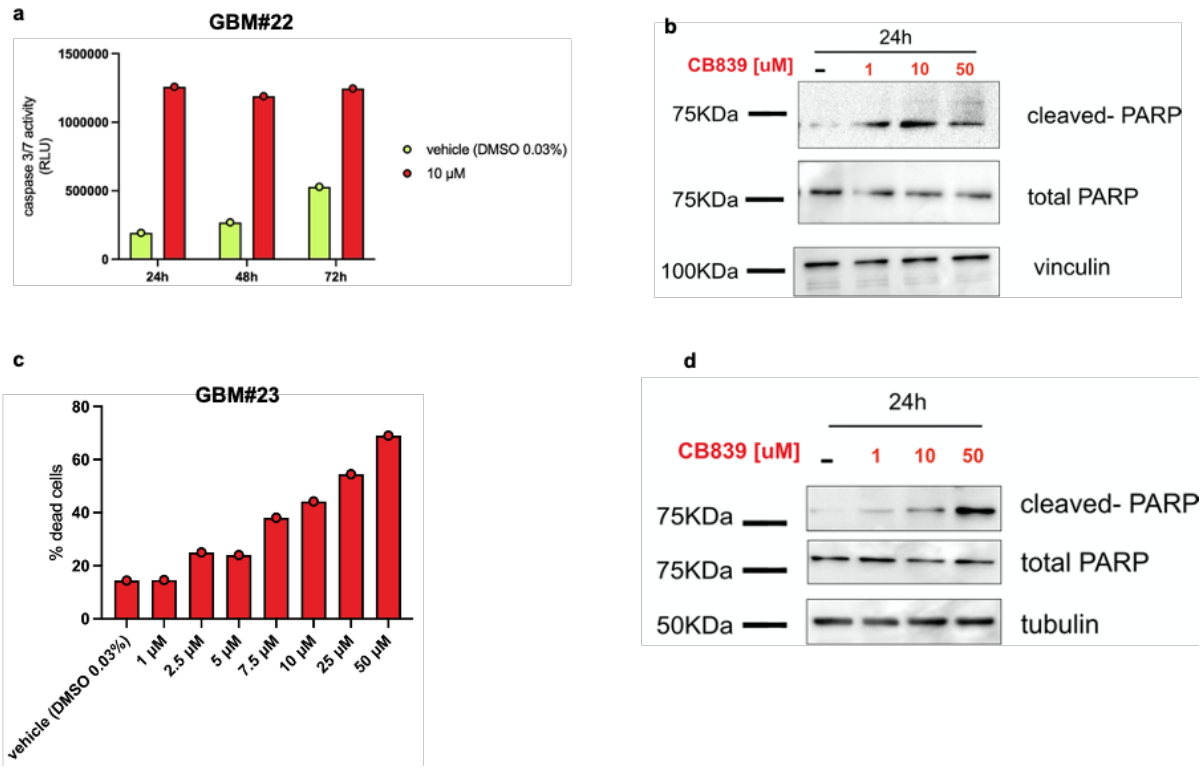


**Figure 16** ***Apoptosis of LSD1i$^{sens}$ and LSD1i$^{res}$ GBM-TICs after CB-839 treatment***. ***a.*** *Caspase 3/7 activity of GBM#22 is evaluated after 24,48,72h in culture with 10µM of CB-839. Results show one experiment, expressed as mean of 5 technical replicates. 0,03% DMSO is used as vehicle.* ***b.*** *Western blot of apoptotic proteins (cleaved PARP vs total PARP) in GBM#22 after CB-839 administration. Vinculin was used for normalization.* ***c.*** *GBM#23 dead cells percentage after CB-839 treatment. Cells viability was evaluated after 72h in culture with different doses of CB-839. Results show one experiment, expressed as mean of 3 technical replicates. 0,03% DMSO is used as vehicle.* ***d.*** *Western blot of apoptotic proteins (cleaved PARP vs total PARP) in GBM#23 after CB-839 administration. Tubulin was used for normalization.*

# 6. DISCUSSION AND FUTURE PROSPECTIVES

In this study, we assessed the role of GLS as a potential driver of LSD1i resistance. GLS was identified through high-throughput synthetic lethal shRNA screening among a setting of metabolic genes. Our aim was to exploit metabolic pathways in GBM TICs as points of vulnerability to sensitize LSD1i-resistant cells to LSD1-directed therapy.

GLS is a mitochondrial enzyme involved in the first step of glutaminolysis. Several studies have demonstrated that glutaminolysis plays a pivotal role in cancer cell metabolism, cell signaling, and cell growth. Increased glutamine metabolism is considered a hallmark of cancer [69,136]. Interestingly, glutaminase isoenzymes (GLS and GLS2) have contrasting functions in tumorigenesis. *In vitro* studies correlate GLS with tumor growth rate and malignancy, and it is regulated by the oncoprotein c-Myc; whereas GLS2 displays tumor suppressive features, and is regulated by p53.[76,87,137,138]

GLS has two isoforms: KGA (long transcript), and GAC (short transcript). GAC has greater catalytic activity and is frequently upregulated in cancer cells. [66,73]

Our protein and mRNA expression analysis results highlighted that GAC isoform is more highly expressed than KGA isoform in both GBM-TIC cohorts (LSD1i$^{sens}$ and LSD1i$^{res}$ TICs). Elevated GAC expression in tumor cells correlates with increased glutaminolysis, contributing to high expression of oncogenes, such as c-Myc, which are involved in tumor progression [25,79].

By analyzing the impact of glutamine addiction, we showed that LSD1i$^{res}$ TICs depend significantly on glutamine when grown under reduced GLN conditions. In contrast, LSD1i$^{sens}$ TICs primarily rely on glucose metabolism, as supported by our unpublished data.

Moreover, we investigated how GLS inhibition affects the proliferation of GBM-TIC cohorts (LSD1i$^{sens}$ and LSD1i$^{res}$ TICs). We employed two different approaches to target GLS: gene silencing and using pharmacological inhibitor which acts directly the protein.

GLS silencing in LSD1$^{res}$ cells reduced their proliferation rate compared to LSD1i$^{sens}$ cells. This suppression in LSD1i$^{sens}$ TICs confirmed their independence from glutamine, whereas LSD1i$^{res}$ TICs showed inhibited proliferation under the same conditions.

Notably, we observed no significant increase in cell death in LSD1i$^{res}$ following GLS silencing. Therefore, we hypothesize that GLS silencing in LSD1i$^{res}$ TICs could induce cell cycle arrest, thereby blocking cell proliferation.

The behavior of LSD1i$^{res}$ cells aligns with the findings of Restall *et al.* where GLS inhibition led to growth blockade and decreased of neurosphere formation in certain GBM patient-derived TICs [139].

Previous studies on GBM stem cells indicated that glutamine depletion or GLS inhibition resulted in either no effect or a modest decrease in cell growth or viability[46,140–142] Interestingly, in the study by Tardito and colleagues [140], which observed no reduction in GBM stem cells growth when cultured without glutamine, it was reported that glutamate uptake from the media occured in all three of the GBM stem cell lines tested. Therefore, understanding the critical role of glutamate in the two GBM-TIC cohorts (LSD1i$^{res}$ and LSD1i$^{sens}$) is potentially essential.

The explanation for the different response to GLS silencing lies in our recent findings on the metabolic flexibility of LSD1i$^{res}$ cells compared to their sensitive counterparts (LSD1i$^{sens}$). These results demonstrate the efficient restoration of cellular homeostasis after stress. In details, LSD1i$^{sens}$ TICs rely predominately on glycolysis and exhibit higher glucose uptake and extracellular acidification rates, suggesting glycolytic dependency.

Conversely, LSD1i$^{res}$ TICs do not show a major metabolic dependency; our proteomic and transcriptomic analyses reveal enrichment in pathways related to ER-Golgi trafficking and protein folding (unpublished data).

To target GLS, we sought to assess the pharmacological potential of CB-839, a promising inhibitor of glutaminolysis. CB-839 is currently undergoing clinical trials to explore its efficacy in cancer therapy[143,144]. However, *in vivo* therapy studies with this drug candidate have shown that its accumulation in the brain is significantly lower compared to other tissues, likely due to difficulties in crossing the BBB[117].

Furthermore, these *in vivo* studies highlight the need to enhance the overall bioavailability of CB-839 at tumor sites, as oral administration requires very high doses to achieve therapeutic efficacy. Therefore, new strategies are urgently needed to ensure more effective delivery of this promising drug candidate to tumor cells.

Notably, CB-839 reduces cellular proliferation in both GBM-TIC cohorts in a dose-response manner. It is also noteworthy that pharmacological inhibition reduces residual catalytic GLS activity approximately of 50%.

This GLS inhibitor has been investigated in solid tumors and in AML, diffuse large B-cell lymphoma, and multiple myeloma cells either alone or in combination with other anticancer drugs [69,134,145–150] .

The inhibition of GLS *in vitro* decreased the levels of downstream glutaminase metabolites (including glutamate, a-ketoglutarate, aspartate, fumarate, and malate) and induced apoptosis [69,145]. Administration of CB-839 in both GBM-TICs cohorts stimulated apoptotic pathways as evidenced by the activation of 3/7 caspase and the presence of cleaved PARP.

Further research and clinical validation of these approaches could lead to improved treatment outcomes for GBM patients. To elucidate the impact of glutamine dependency on LSD1i responsiveness, we are planning to employ real-time assays (Seahorse) to measure energy metabolism in live cells. Additionally, to investigate the decrease of cellular growth in GLS-silenced LSD1i$^{res}$ cells, we will analyze the cell cycle using flow cytometry and immunofluorescence. Moreover, we intend to assess *in vivo* tumorigenicity of both control and GLS silenced TICs, specifically evaluating the effects of GLS silencing (or its pharmacological inhibition) and LSD1i treatment on GBM-PDXs.

In conclusion, our study underscores the importance of GLS in the metabolic adaptation of GBM-TICs, particularly those resistant to LSD1i. Targeting GLS, either alone or in combination with LSD1i, presents a promising strategy to disrupt the metabolic flexibility that supports tumor growth and resistance.

# 7. BIBLIOGRAPHY


1. Ostrom, Q. T. *et al*. CBTRUS Statistical Report: Primary Brain and Other Central Nervous System Tumors Diagnosed in the United States in 2013-2017. *Neuro Oncol* **22**, IV1–IV96 (2020).
2. Jiang, H., Cui, Y., Wang, J. & Lin, S. Impact of epidemiological characteristics of supratentorial gliomas in adults brought about by the 2016 world health organization classification of tumors of the central nervous system. *Oncotarget* **8**, 20354–20361 (2017).
3. Hanif, F., Muzaffar, K., Perveen, K., Malhi, S. M. & Simjee, S. U. Glioblastoma Multiforme: A Review of its Epidemiology and Pathogenesis through Clinical Presentation and Treatment. *Asian Pac J Cancer Prev* **18**, 3 (2017).
4. Okamoto, Y. *et al*. Population-based study on incidence, survival rates, and genetic alterations of low-grade diffuse astrocytomas and oligodendrogliomas. *Acta Neuropathol* **108**, 49–56 (2004).
5. Brain Tumor Epidemiology: Consensus from the Brain Tumor Epidemiology Consortium (BTEC) - PMC. https://www.ncbi.nlm.nih.gov/pmc/articles/PMC2861559/.
6. Linos, E., Raine, T., Alonso, A. & Michaud, D. Atopy and risk of brain tumors: a meta-analysis. *J Natl Cancer Inst* **99**, 1544–1550 (2007).
7. Sadetzki, S. *et al*. Genotyping of patients with sporadic and radiation-associated meningiomas. *Cancer Epidemiol Biomarkers Prev* **14**, 969–976 (2005).
8. Chitnis, S., Hosseini, R. & Xie, P. Brain tumor classification based on neural architecture search. *Sci Rep* **12**, 19206 (2022).
9. Nakada, M. *et al*. Aberrant signaling pathways in glioma. *Cancers (Basel)* **3**, 3242–3278 (2011).
10. Smith, C. & Ironside, J. W. Diagnosis and pathogenesis of gliomas. *Curr Diagn Pathol* **13**, 180–192 (2007).
11. LN, G. C. & P, W. The cIMPACT-NOW updates and their significance to current neuro-oncology practice. *Neurooncol Pract* **8**, 4–10 (2020).
12. Louis, D. N. *et al*. The 2021 WHO Classification of Tumors of the Central Nervous System: a summary. *Neuro Oncol* **23**, 1231–1251 (2021).
13. Stoyanov, G. S. *et al*. Reclassification of Glioblastoma Multiforme According to the 2021 World Health Organization Classification of Central Nervous System Tumors: A Single Institution Report and Practical Significance. *Cureus* **14**, (2022).
14. Brat, D. J. *et al*. Molecular Biomarker Testing for the Diagnosis of Diffuse Gliomas. *Arch Pathol Lab Med* **146**, 547–574 (2022).
15. Berger, T. R., Wen, P. Y., Lang-Orsini, M. & Chukwueke, U. N. World Health Organization 2021 Classification of Central Nervous System Tumors and Implications for Therapy for Adult-Type Gliomas: A Review. *JAMA Oncol* **8**, 1493–1501 (2022).
16. Ramos-Fresnedo, A. *et al*. The survival outcomes of molecular glioblastoma IDH-wildtype: a multicenter study. *J Neurooncol* **157**, 177–185 (2022).
17. Horbinski, C., Berger, T., Packer, R. J. & Wen, P. Y. Clinical implications of the 2021 edition of the WHO classification of central nervous system tumours. *Nat Rev Neurol* **18**, 515–529 (2022).
18. Park, Y. W. *et al*. The 2021 WHO Classification for Gliomas and Implications on Imaging Diagnosis: Part 1—Key Points of the Fifth Edition and Summary of Imaging

Findings on Adult-Type Diffuse Gliomas. *Journal of Magnetic Resonance Imaging* **58**, 677–689 (2023).
19. Tesileanu, C. M. S. *et al*. Survival of diffuse astrocytic glioma, IDH1/2 wildtype, with molecular features of glioblastoma, WHO grade IV: a confirmation of the cIMPACT-NOW criteria. *Neuro Oncol* **22**, 515–523 (2020).
20. Guo, X. *et al*. Histological and molecular glioblastoma, IDH-wildtype: a real-world landscape using the 2021 WHO classification of central nervous system tumors. *Front Oncol* **13**, (2023).
21. Komori, T. Grading of adult diffuse gliomas according to the 2021 WHO Classification of Tumors of the Central Nervous System. *Lab Invest* **102**, 126–133 (2022).
22. Stupp, R. *et al*. Radiotherapy plus concomitant and adjuvant temozolomide for glioblastoma. *N Engl J Med* **352**, 987–996 (2005).
23. Weller, M. *et al*. EANO guideline for the diagnosis and treatment of anaplastic gliomas and glioblastoma. *Lancet Oncol* **15**, (2014).
24. Chen, J. *et al*. A restricted cell population propagates glioblastoma growth following chemotherapy. *Nature* **488**, 522 (2012).
25. Wang, J. *et al*. c-Myc Is Required for Maintenance of Glioma Cancer Stem Cells. *PLoS One* **3**, (2008).
26. Poon, M. T. C., Sudlow, C. L. M., Figueroa, J. D. & Brennan, P. M. Longer-term (≥ 2 years) survival in patients with glioblastoma in population-based studies pre- and post-2005: a systematic review and meta-analysis. *Sci Rep* **10**, (2020).
27. Ostrom, Q. T. *et al*. The epidemiology of glioma in adults: a 'state of the science' review. *Neuro Oncol* **16**, 896–913 (2014).
28. Sottoriva, A. *et al*. Intratumor heterogeneity in human glioblastoma reflects cancer evolutionary dynamics. *Proc Natl Acad Sci U S A* **110**, 4009–4014 (2013).
29. Patel, A. P. *et al*. Single-cell RNA-seq highlights intratumoral heterogeneity in primary glioblastoma. *Science* **344**, 1396–1401 (2014).
30. Neftel, C. *et al*. An Integrative Model of Cellular States, Plasticity, and Genetics for Glioblastoma. *Cell* **178**, 835-849.e21 (2019).
31. Bhaduri, A. *et al*. Outer Radial Glia-like Cancer Stem Cells Contribute to Heterogeneity of Glioblastoma. *Cell Stem Cell* **26**, 48-63.e6 (2020).
32. Guilhamon, P. *et al*. Single-cell chromatin accessibility profiling of glioblastoma identifies an invasive cancer stem cell population associated with lower survival. *Elife* **10**, 1–20 (2021).
33. Wang, Q. *et al*. Tumor Evolution of Glioma-Intrinsic Gene Expression Subtypes Associates with Immunological Changes in the Microenvironment. *Cancer Cell* **32**, 42-56.e6 (2017).
34. Richards, L. M. *et al*. Gradient of Developmental and Injury Response transcriptional states defines functional vulnerabilities underpinning glioblastoma heterogeneity. *Nat Cancer* **2**, 157–173 (2021).
35. Garofano, L. *et al*. Pathway-based classification of glioblastoma uncovers a mitochondrial subtype with therapeutic vulnerabilities. *Nat Cancer* **2**, 141–156 (2021).
36. Richards, L. M. *et al*. Gradient of Developmental and Injury Response transcriptional states defines functional vulnerabilities underpinning glioblastoma heterogeneity. *Nat Cancer* **2**, 157–173 (2021).
37. Singh, S. K. *et al*. Identification of human brain tumour initiating cells. *Nature* **432**, 396–401 (2004).

38. Reya, T., Morrison, S. J., Clarke, M. F. & Weissman, I. L. Stem cells, cancer, and cancer stem cells. *Nature* **414**, 105–111 (2001).
39. Bonnet, D. & Dick, J. E. Human acute myeloid leukemia is organized as a hierarchy that originates from a primitive hematopoietic cell. *Nat Med* **3**, 730–737 (1997).
40. Meacham, C. E. & Morrison, S. J. Tumour heterogeneity and cancer cell plasticity. *Nature* **501**, 328–337 (2013).
41. Heiden, M. G. V., Cantley, L. C. & Thompson, C. B. Understanding the Warburg Effect: The Metabolic Requirements of Cell Proliferation. *Science* **324**, 1029 (2009).
42. Oudard, S. *et al.* High glycolysis in gliomas despite low hexokinase transcription and activity correlated to chromosome 10 loss. *Br J Cancer* **74**, 839 (1996).
43. La Fougère, C., Suchorska, B., Bartenstein, P., Kreth, F. W. & Tonn, J. C. Molecular imaging of gliomas with PET: opportunities and limitations. *Neuro Oncol* **13**, 806–819 (2011).
44. Costanzo, A. *et al.* Proton MR spectroscopy of cerebral gliomas at 3 T: spatial heterogeneity, and tumour grade and extent. *Eur Radiol* **18**, 1727–1735 (2008).
45. Maher, E. A. *et al.* Metabolism of [U-13 C]glucose in human brain tumors in vivo. *NMR Biomed* **25**, 1234–1244 (2012).
46. Marin-Valencia, I. *et al.* Analysis of tumor metabolism reveals mitochondrial glucose oxidation in genetically diverse human glioblastomas in the mouse brain in vivo. *Cell Metab* **15**, 827–837 (2012).
47. May, J. L. *et al.* IDH3α regulates one-carbon metabolism in glioblastoma. *Sci Adv* **5**, (2019).
48. Izquierdo-Garcia, J. L. *et al.* Glioma cells with the IDH1 mutation modulate metabolic fractional flux through pyruvate carboxylase. *PLoS One* **9**, (2014).
49. Singh, D. *et al.* Transforming fusions of FGFR and TACC genes in human glioblastoma. *Science* **337**, 1231–1235 (2012).
50. Frattini, V. *et al.* A metabolic function of FGFR3-TACC3 gene fusions in cancer. *Nature* **553**, 222–227 (2018).
51. Hoang-Minh, L. B. *et al.* Infiltrative and drug-resistant slow-cycling cells support metabolic heterogeneity in glioblastoma. *EMBO J* **37**, (2018).
52. Marin-Valencia, I. *et al.* Analysis of tumor metabolism reveals mitochondrial glucose oxidation in genetically diverse human glioblastomas in the mouse brain in vivo. *Cell Metab* **15**, 827–837 (2012).
53. Vlashi, E. *et al.* Metabolic state of glioma stem cells and nontumorigenic cells. *Proc Natl Acad Sci U S A* **108**, 16062–16067 (2011).
54. Saga, I. *et al.* Integrated analysis identifies different metabolic signatures for tumor-initiating cells in a murine glioblastoma model. *Neuro Oncol* **16**, 1048–1056 (2014).
55. Sanzey, M. *et al.* Comprehensive analysis of glycolytic enzymes as therapeutic targets in the treatment of glioblastoma. *PLoS One* **10**, (2015).
56. Janiszewska, M. *et al.* Imp2 controls oxidative phosphorylation and is crucial for preserving glioblastoma cancer stem cells. *Genes Dev* **26**, 1926–1944 (2012).
57. Park, H. K. *et al.* Interplay between TRAP1 and Sirtuin-3 Modulates Mitochondrial Respiration and Oxidative Stress to Maintain Stemness of Glioma Stem Cells. *Cancer Res* **79**, 1369–1382 (2019).
58. Puca, F. *et al.* Medium-Chain Acyl-CoA Dehydrogenase Protects Mitochondria from Lipid Peroxidation in Glioblastoma. *Cancer Discov* **11**, 2904–2923 (2021).
59. Lin, H. *et al.* Fatty acid oxidation is required for the respiration and proliferation of malignant glioma cells. *Neuro Oncol* **19**, 43–54 (2017).

60. Oizel, K. *et al*. Efficient Mitochondrial Glutamine Targeting Prevails Over Glioblastoma Metabolic Plasticity. *Clin Cancer Res* **23**, 6292–6305 (2017).
61. Chen, C. *et al*. ATF4-dependent fructolysis fuels growth of glioblastoma multiforme. *Nat Commun* **13**, (2022).
62. Márquez, J., López de la Oliva, A. R., Matés, J. M., Segura, J. A. & Alonso, F. J. Glutaminase: a multifaceted protein not only involved in generating glutamate. *Neurochem Int* **48**, 465–471 (2006).
63. Chung-Bok, M. Il, Vincent, N., Jhala, U. & Watford, M. Rat hepatic glutaminase: Identification of the full coding sequence and characterization of a functional promoter. *Biochemical Journal* **324**, 193–200 (1997).
64. Pérez-Gómez, C. *et al*. Genomic organization and transcriptional analysis of the human l-glutaminase gene. *Biochem J* **370**, 771–784 (2003).
65. Aledo, J. C., Gómez-Fabre, P. M., Olalla, L. & Márquez, J. Identification of two human glutaminase loci and tissue-specific expression of the two related genes. *Mamm Genome* **11**, 1107–1110 (2000).
66. Elgadi, K. M., Meguid, R. A., Qian, M., Souba, W. W. & Abcouwer, S. F. Cloning and analysis of unique human glutaminase isoforms generated by tissue-specific alternative splicing. *Physiol Genomics* **1**, 51–62 (1999).
67. Porter, L. D., Ibrahim, H., Taylor, L. & Curthoys, N. P. Complexity and species variation of the kidney-type glutaminase gene. *Physiol Genomics* **9**, 157–166 (2002).
68. Morehouse, R. F. & Curthoys, N. P. Properties of rat renal phosphate-dependent glutaminase coupled to Sepharose. Evidence that dimerization is essential for activation. *Biochem J* **193**, 709–716 (1981).
69. Jacque, N. *et al*. Targeting glutaminolysis has antileukemic activity in acute myeloid leukemia and synergizes with BCL-2 inhibition. *Blood* **126**, 1346–1356 (2015).
70. Morehouse, R. F. & Curthoys, N. P. Properties of rat renal phosphate-dependent glutaminase coupled to Sepharose. Evidence that dimerization is essential for activation. *Biochem J* **193**, 709–716 (1981).
71. Cassago, A. *et al*. Mitochondrial localization and structure-based phosphate activation mechanism of Glutaminase C with implications for cancer metabolism. *Proc Natl Acad Sci U S A* **109**, 1092–1097 (2012).
72. Yu, D. *et al*. Kidney-type glutaminase (GLS1) is a biomarker for pathologic diagnosis and prognosis of hepatocellular carcinoma. *Oncotarget* **6**, 7619 (2015).
73. Cassago, A. *et al*. Mitochondrial localization and structure-based phosphate activation mechanism of Glutaminase C with implications for cancer metabolism. *Proc Natl Acad Sci U S A* **109**, 1092–1097 (2012).
74. Elgadi, K. M., Meguid, R. A., Qian, M., Souba, W. W. & Abcouwer, S. F. Cloning and analysis of unique human glutaminase isoforms generated by tissue-specific alternative splicing. *Physiol Genomics* **1**, 51–62 (1999).
75. Szeliga, M. *et al*. Relative expression of mRNAS coding for glutaminase isoforms in CNS tissues and CNS tumors. *Neurochem Res* **33**, 808–813 (2008).
76. Szeliga, M. *et al*. Silencing of GLS and overexpression of GLS2 genes cooperate in decreasing the proliferation and viability of glioblastoma cells. *Tumour Biol* **35**, 1855–1862 (2014).
77. Turner, A. & McGivan, J. D. Glutaminase isoform expression in cell lines derived from human colorectal adenomas and carcinomas. *Biochem J* **370**, 403–408 (2003).

78. Kan, C. C., Chung, T. Y., Wu, H. Y., Juo, Y. A. & Hsieh, M. H. Exogenous glutamate rapidly induces the expression of genes involved in metabolism and defense responses in rice roots. *BMC Genomics* **18**, (2017).
79. Wang, J. Bin *et al*. Targeting mitochondrial glutaminase activity inhibits oncogenic transformation. *Cancer Cell* **18**, 207–219 (2010).
80. Martins, F., Gonçalves, L. G., Pojo, M. & Serpa, J. Take Advantage of Glutamine Anaplerosis, the Kernel of the Metabolic Rewiring in Malignant Gliomas. *Biomolecules* **10**, 1–25 (2020).
81. Ahluwalia, G. S., Grem, J. L., Hao, Z. & Cooney, D. A. Metabolism and action of amino acid analog anti-cancer agents. *Pharmacol Ther* **46**, 243–271 (1990).
82. Thangavelu, K. *et al*. Structural basis for the allosteric inhibitory mechanism of human kidney-type glutaminase (KGA) and its regulation by Raf-Mek-Erk signaling in cancer cell metabolism. *Proc Natl Acad Sci U S A* **109**, 7705–7710 (2012).
83. Ascenção, C. F. R. *et al*. N-terminal phosphorylation of glutaminase C decreases its enzymatic activity and cancer cell migration. *Biochimie* **154**, 69–76 (2018).
84. Han, T. *et al*. Phosphorylation of glutaminase by PKCε is essential for its enzymatic activity and critically contributes to tumorigenesis. *Cell Res* **28**, 655–669 (2018).
85. Ascenção, C. F. R. *et al*. N-terminal phosphorylation of glutaminase C decreases its enzymatic activity and cancer cell migration. *Biochimie* **154**, 69–76 (2018).
86. Matés, J. M., Campos-Sandoval, J. A., de los Santos-Jiménez, J. & Márquez, J. Glutaminases regulate glutathione and oxidative stress in cancer. *Archives of Toxicology* vol. 94 2603–2623 Preprint at https://doi.org/10.1007/s00204-020-02838-8 (2020).
87. Katt, W. P., Lukey, M. J. & Cerione, R. A. A tale of two glutaminases: homologous enzymes with distinct roles in tumorigenesis. *Future Med Chem* **9**, 223–243 (2017).
88. Suzuki, S. *et al*. Phosphate-activated glutaminase (GLS2), a p53-inducible regulator of glutamine metabolism and reactive oxygen species. *Proc Natl Acad Sci U S A* **107**, 7461–7466 (2010).
89. Hu, W. *et al*. Glutaminase 2, a novel p53 target gene regulating energy metabolism and antioxidant function. *Proc Natl Acad Sci U S A* **107**, 7455–7460 (2010).
90. Hu, W. *et al*. Glutaminase 2, a novel p53 target gene regulating energy metabolism and antioxidant function. *Proc Natl Acad Sci U S A* **107**, 7455–7460 (2010).
91. Moreira Franco, Y. E. *et al*. Glutaminolysis dynamics during astrocytoma progression correlates with tumor aggressiveness. *Cancer Metab* **9**, (2021).
92. Gao, P. *et al*. c-Myc suppression of miR-23a/b enhances mitochondrial glutaminase expression and glutamine metabolism. *Nature* **458**, 762–765 (2009).
93. Márquez, J. *et al*. Glutamine Addiction In Gliomas. *Neurochem Res* **42**, 1735–1746 (2017).
94. Lv, H. *et al*. Unraveling the Potential Role of Glutathione in Multiple Forms of Cell Death in Cancer Therapy. *Oxid Med Cell Longev* **2019**, (2019).
95. Wang, Z. *et al*. Pseudolaric acid B triggers ferroptosis in glioma cells via activation of Nox4 and inhibition of xCT. *Cancer Lett* **428**, 21–33 (2018).
96. Oruganty, K., Campit, S. E., Mamde, S., Lyssiotis, C. A. & Chandrasekaran, S. Common biochemical properties of metabolic genes recurrently dysregulated in tumors. *Cancer Metab* **8**, (2020).
97. Olalla, L. *et al*. Nuclear localization of L-type glutaminase in mammalian brain. *J Biol Chem* **277**, 38939–38944 (2002).

98. Eagle, H. METABOLIC CONTROLS IN CULTURED MAMMALIAN CELLS. *Science* **148**, 42–51 (1965).
99. DeBerardinis, R. J., Lum, J. J., Hatzivassiliou, G. & Thompson, C. B. The biology of cancer: metabolic reprogramming fuels cell growth and proliferation. *Cell Metab* **7**, 11–20 (2008).
100. Lunt, S. Y. & Vander Heiden, M. G. Aerobic glycolysis: meeting the metabolic requirements of cell proliferation. *Annu Rev Cell Dev Biol* **27**, 441–464 (2011).
101. Wise, D. R. & Thompson, C. B. Glutamine addiction: a new therapeutic target in cancer. *Trends Biochem Sci* **35**, 427–433 (2010).
102. Cacace, A., Sboarina, M., Vazeille, T. & Sonveaux, P. Glutamine activates STAT3 to control cancer cell proliferation independently of glutamine metabolism. *Oncogene* **36**, 2074–2084 (2017).
103. Vučetić, M., Cormerais, Y., Parks, S. K. & Pouysségur, J. The Central Role of Amino Acids in Cancer Redox Homeostasis: Vulnerability Points of the Cancer Redox Code. *Front Oncol* **7**, (2017).
104. Bhutia, Y. D., Babu, E., Ramachandran, S. & Ganapathy, V. Amino Acid transporters in cancer and their relevance to 'glutamine addiction': novel targets for the design of a new class of anticancer drugs. *Cancer Res* **75**, 1782–1788 (2015).
105. Hoerner, C. R., Chen, V. J. & Fan, A. C. The 'Achilles Heel' of Metabolism in Renal Cell Carcinoma: Glutaminase Inhibition as a Rational Treatment Strategy. *Kidney Cancer* **3**, 15–29 (2019).
106. Durán, R. V. *et al*. Glutaminolysis activates Rag-mTORC1 signaling. *Mol Cell* **47**, 349–358 (2012).
107. Csibi, A. *et al*. The mTORC1/S6K1 pathway regulates glutamine metabolism through the eif4b-dependent control of c-Myc translation. *Current Biology* **24**, 2274–2280 (2014).
108. Nicklin, P. *et al*. Bidirectional transport of amino acids regulates mTOR and autophagy. *Cell* **136**, 521–534 (2009).
109. Robinson, M. M. *et al*. Novel mechanism of inhibition of rat kidney-type glutaminase by bis-2-(5-phenylacetamido-1,2,4-thiadiazol-2-yl)ethyl sulfide (BPTES). *Biochem J* **406**, 407–414 (2007).
110. Zimmermann, S. C. *et al*. Allosteric Glutaminase Inhibitors Based on a 1,4-Di(5-amino-1,3,4-thiadiazol-2-yl)butane Scaffold. *ACS Med Chem Lett* **7**, 520–524 (2016).
111. Seltzer, M. J. *et al*. Inhibition of glutaminase preferentially slows growth of glioma cells with mutant IDH1. *Cancer Res* **70**, 8981–8987 (2010).
112. Lee, Y. Z. *et al*. Discovery of selective inhibitors of Glutaminase-2, which inhibit mTORC1, activate autophagy and inhibit proliferation in cancer cells. *Oncotarget* **5**, 6087 (2014).
113. Katt, W. P., Ramachandran, S., Erickson, J. W. & Cerione, R. A. Dibenzophenanthridines as inhibitors of glutaminase C and cancer cell proliferation. *Mol Cancer Ther* **11**, 1269–1278 (2012).
114. Yuan, L. *et al*. Glutaminase inhibitor compound 968 inhibits cell proliferation and sensitizes paclitaxel in ovarian cancer. *Am J Transl Res* **8**, 4265 (2016).
115. Berkers, C. R., Maddocks, O. D. K., Cheung, E. C., Mor, I. & Vousden, K. H. Metabolic Regulation by p53 Family Members. *Cell Metab* **18**, 617 (2013).
116. Gross, M. I. *et al*. Antitumor activity of the glutaminase inhibitor CB-839 in triple-negative breast cancer. *Mol Cancer Ther* **13**, 890–901 (2014).

117. Gross, M. I. *et al*. Antitumor activity of the glutaminase inhibitor CB-839 in triple-negative breast cancer. *Mol Cancer Ther* **13**, 890–901 (2014).
118. Maeda, H., Nakamura, H. & Fang, J. The EPR effect for macromolecular drug delivery to solid tumors: Improvement of tumor uptake, lowering of systemic toxicity, and distinct tumor imaging in vivo. *Adv Drug Deliv Rev* **65**, 71–79 (2013).
119. Giesen, B., Nickel, A.-C., Barthel, J., Kahlert, D. & Janiak, C. pharmaceutics Augmented Therapeutic Potential of Glutaminase Inhibitor CB839 in Glioblastoma Stem Cells Using Gold Nanoparticle Delivery. (2021) doi:10.3390/pharmaceutics13020295.
120. Huang, Q. *et al*. Characterization of the interactions of potent allosteric inhibitors with glutaminase C, a key enzyme in cancer cell glutamine metabolism. *J Biol Chem* **293**, 3535 (2018).
121. Masisi, B. K. *et al*. The role of glutaminase in cancer. *Histopathology* vol. 76 498–508 Preprint at https://doi.org/10.1111/his.14014 (2020).
122. Matilainen, O., Quirós, P. M. & Auwerx, J. Mitochondria and Epigenetics - Crosstalk in Homeostasis and Stress. *Trends Cell Biol* **27**, 453–463 (2017).
123. Liu, Y. & Yang, C. Oncometabolites in Cancer: Current Understanding and Challenges. *Cancer Res* **81**, 2820–2823 (2021).
124. Kusi-Mensah, K. *et al*. A Systematic Review of the Validity and Reliability of Assessment Tools for Executive Function and Adaptive Function Following Brain Pathology among Children and Adolescents in Low- and Middle-Income Countries. *Neuropsychol Rev* **32**, 974–1016 (2022).
125. Ward, P. S. *et al*. The common feature of leukemia-associated IDH1 and IDH2 mutations is a neomorphic enzyme activity converting alpha-ketoglutarate to 2-hydroxyglutarate. *Cancer Cell* **17**, 225–234 (2010).
126. Dang, C. V., Hamaker, M., Sun, P., Le, A. & Gao, P. Therapeutic targeting of cancer cell metabolism. *J Mol Med (Berl)* **89**, 205–212 (2011).
127. Xiao, M. *et al*. Inhibition of α-KG-dependent histone and DNA demethylases by fumarate and succinate that are accumulated in mutations of FH and SDH tumor suppressors. *Genes Dev* **26**, 1326–1338 (2012).
128. Letouzé, E. *et al*. SDH mutations establish a hypermethylator phenotype in paraganglioma. *Cancer Cell* **23**, 739–752 (2013).
129. Killian, J. K. *et al*. Recurrent epimutation of SDHC in gastrointestinal stromal tumors. *Sci Transl Med* **6**, 268ra177 (2014).
130. Pietrocola, F., Galluzzi, L., Bravo-San Pedro, J. M., Madeo, F. & Kroemer, G. Acetyl coenzyme A: a central metabolite and second messenger. *Cell Metab* **21**, 805–821 (2015).
131. Teperino, R. *et al*. Hedgehog partial agonism drives Warburg-like metabolism in muscle and brown fat. *Cell* **151**, 414–426 (2012).
132. Betto, R. M. *et al*. Metabolic control of DNA methylation in naive pluripotent cells. *Nat Genet* **53**, 215–229 (2021).
133. Faletti, S. *et al*. LSD1-directed therapy affects glioblastoma tumorigenicity by deregulating the protective ATF4-dependent integrated stress response. *Sci Transl Med* **13**, (2021).
134. Wicker, C. A. *et al*. Glutaminase inhibition with telaglenastat (CB-839) improves treatment response in combination with ionizing radiation in head and neck squamous cell carcinoma models. *Cancer Lett* **502**, 180–188 (2021).

135. Harding, J. J. *et al*. A phase I dose-escalation and expansion study of telaglenastat in patients with advanced or metastatic solid tumors. *Clinical Cancer Research* **27**, 4994–5003 (2021).
136. Herranz, D. Glutaminolysis gets the spotlight in cancer. *Oncotarget* **8**, 10761 (2017).
137. Suzuki, S. *et al*. Phosphate-activated glutaminase (GLS2), a p53-inducible regulator of glutamine metabolism and reactive oxygen species. *Proc Natl Acad Sci U S A* **107**, 7461–7466 (2010).
138. Hu, W. *et al*. Glutaminase 2, a novel p53 target gene regulating energy metabolism and antioxidant function. *Proc Natl Acad Sci U S A* **107**, 7455–7460 (2010).
139. Restall, I. J. *et al*. Brain Tumor Stem Cell Dependence on Glutaminase Reveals a Metabolic Vulnerability through the Amino Acid Deprivation Response Pathway. *Cancer Res* **80**, 5478–5490 (2020).
140. Tardito, S. *et al*. Glutamine synthetase activity fuels nucleotide biosynthesis and supports growth of glutamine-restricted glioblastoma. *Nat Cell Biol* **17**, 1556–1568 (2015).
141. Kahlert, U. D. *et al*. Alterations in cellular metabolome after pharmacological inhibition of Notch in glioblastoma cells. *Int J Cancer* **138**, 1246–1255 (2016).
142. Oizel, K. *et al*. Efficient Mitochondrial Glutamine Targeting Prevails Over Glioblastoma Metabolic Plasticity. *Clin Cancer Res* **23**, 6292–6305 (2017).
143. Giesen, B., Nickel, A. C., Barthel, J., Kahlert, U. D. & Janiak, C. Augmented Therapeutic Potential of Glutaminase Inhibitor CB839 in Glioblastoma Stem Cells Using Gold Nanoparticle Delivery. *Pharmaceutics* **13**, 1–18 (2021).
144. Study of CB-839 in Combination w/ Paclitaxel in Participants of African Ancestry and Non-African Ancestry With Advanced Triple Negative Breast Cancer (TNBC) - Full Text View - ClinicalTrials.gov. https://classic.clinicaltrials.gov/ct2/show/NCT03057600.
145. Matre, P. *et al*. Inhibiting glutaminase in acute myeloid leukemia: metabolic dependency of selected AML subtypes. *Oncotarget* **7**, 79722–79735 (2016).
146. Dos Reis, L. M. *et al*. Dual inhibition of glutaminase and carnitine palmitoyltransferase decreases growth and migration of glutaminase inhibition-resistant triple-negative breast cancer cells. *J Biol Chem* **294**, 9342–9357 (2019).
147. Wicker, C. A. *et al*. Glutaminase inhibition with telaglenastat (CB-839) improves treatment response in combination with ionizing radiation in head and neck squamous cell carcinoma models. *Cancer Lett* **502**, 180–188 (2021).
148. Zavorka Thomas, M. E. *et al*. Gilteritinib Inhibits Glutamine Uptake and Utilization in FLT3-ITD-Positive AML. *Mol Cancer Ther* **20**, 2207–2217 (2021).
149. Thompson, R. M. *et al*. Glutaminase inhibitor CB-839 synergizes with carfilzomib in resistant multiple myeloma cells. *Oncotarget* **8**, 35863–35876 (2017).
150. Gross, M. I. *et al*. Antitumor activity of the glutaminase inhibitor CB-839 in triple-negative breast cancer. *Mol Cancer Ther* **13**, 890–901 (2014).